POLITECNICO DI TORINO
Repository ISTITUZIONALE

Evidence of Nuclear Geometry-Driven Anisotropic Flow in O+O and Ne+Ne Collisions at NN=5.36TeV

Original
Evidence of Nuclear Geometry-Driven Anisotropic Flow in O+O and Ne+Ne Collisions at NN=5.36TeV / Abualrob, I.j., Acharya, S., Aglieri Rinella, G., Aglietta, L., Agrawal, N., Ahammed, Z., Ahmad, S., Ahuja, I., Akbar, Z., Akindinov, A., Akishina, V., Al-Turany, M., Aleksandrov, D., Alessandro, B., Alfaro Molina, R., Ali, B., Alici, A., Alkin, A., Alme, J., Alocco, G., et al.. - In: PHYSICAL REVIEW LETTERS. - ISSN 0031-9007. - 137:8(2026). [10.1103/gymp-vp87]

Availability:
This version is available at: 11583/3016100 since: 2026-09-29T20:25:26Z

Publisher:
APS

Published
DOI:10.1103/gymp-vp87

Terms of use:

This article is made available under terms and conditions as specified in the corresponding bibliographic description in the repository

Publisher copyright

(Article begins on next page)

22 November 2026

Editors' Suggestion

Evidence of Nuclear Geometry-Driven Anisotropic Flow in O + O and Ne + Ne Collisions at $\sqrt{s_{\mathrm{NN}}} = 5.36$ TeV

I. J. Abualrob *et al.*[*]
(ALICE Collaboration)

(Received 18 September 2025; revised 10 February 2026; accepted 15 May 2026; published 17 August 2026)

A central question in strong-interaction physics, governed by quantum chromodynamics (QCD), is whether femtoscale droplets of quark-gluon plasma form in small collision systems involving projectiles significantly smaller than heavy ions. Collisions of light ions such as ^{16}O and ^{20}Ne offer a unique opportunity to probe the emergence of collective behavior in QCD matter. This Letter presents the first measurements of the elliptic (v_2) and triangular (v_3) flow of charged particles in ^{16}O–^{16}O and ^{20}Ne–^{20}Ne collisions at a center-of-mass energy per nucleon pair of $\sqrt{s_{\mathrm{NN}}} = 5.36$ TeV with the ALICE detector. The hydrodynamic model predictions, explicitly incorporating the nuclear structures of ^{16}O and ^{20}Ne, exhibit a good agreement with the flow measurements presented. The observed increase of v_2 in central Ne–Ne collisions relative to OO collisions, driven by the nuclear geometries, highlights the importance of utilizing light nuclei with well-defined geometric shapes to constrain the initial conditions. These findings support the presence of nuclear geometry-driven hydrodynamic flow in light-ion collisions at the LHC.

DOI: 10.1103/gymp-vp87

The primary goal of ultrarelativistic nuclear collisions is to recreate the quark-gluon plasma (QGP)—a state of matter that is thought to have existed in the early Universe—and to investigate its properties [1–5]. A significant effort has been dedicated to determining the precise properties and time evolution of the QGP. One of the most important approaches is the study of anisotropic flow [6], which arises from the transfer of initial spatial anisotropy to momentum anisotropy in the final state via pressure gradients within the created medium. Anisotropic flow is characterized by the Fourier coefficients v_n of the azimuthal particle distribution,

$$\frac{dN}{d\varphi} \propto 1 + 2\sum_{n=1}^{\infty} v_n \cos[n(\varphi - \Psi_n)], \tag{1}$$

where φ is the azimuthal angle of the final state produced particle, Ψ_n is the nth-order symmetry plane, and v_n are the flow coefficients. Experimental measurements of v_n coefficients and their event-by-event fluctuations, from two-particle and multiparticle correlations with inclusive and identified charged hadrons in heavy-ion collisions, have been performed [7–16]. The measurements can be quantitatively reproduced by hydrodynamic model calculations. This agreement provides strong evidence that the QGP created in heavy-ion collisions at the LHC behaves as a nearly perfect fluid [17–20], characterized by an exceptionally small specific shear viscosity (η/s), which approaches the quantum lower bound of $1/4\pi$ [21].

In addition to colliding heavy ions at ultrarelativistic energies, the LHC also provides pp and p-Pb collisions. The formation of a QGP was not anticipated in these small systems, and they were initially viewed as baselines for heavy-ion collisions [22]. Surprisingly, the experimental results have revealed new manifestations of emergent QCD phenomena, such as finite anisotropic flow in high-multiplicity events [4,11,23–30], with the first indication provided by the observation of a long-range "ridge" in two-particle correlations in pp and p-Pb collisions at the LHC [23–26], in p-Au at RHIC [31,32] and even possible hints in high multiplicity e^+e^- collisions at ALEPH [33]. Subsequent multiparticle correlation measurements confirmed the collective nature of the signal [11,27,28]. Measurements performed in different collision systems, such as p-Au, d-Au, and ^{3}He–Au at RHIC [27,34], as well as pp, p-Pb, and Pb–Pb collisions at the LHC [11,29,30,35–38], revealed that the observed anisotropic flow in small collision systems is predominantly driven by the initial geometry and its event-by-event fluctuations through the complex dynamic evolution of the created system [39–42]. The most recent anisotropic flow measurements for identified hadrons presented results consistent with the formation of partonic collectivity in small systems [35,43].

While hydrodynamic and parton transport models qualitatively describe many of the collective flow features in

[*]Full author list given at the end of the Letter.

Published by the American Physical Society under the terms of the Creative Commons Attribution 4.0 International license. Further distribution of this work must maintain attribution to the author(s) and the published article's title, journal citation, and DOI. Open access publication funded by CERN.

 © 2026 CERN, for the ALICE Collaboration

small collision systems, there are discrepancies, i.e., in the magnitudes of flow coefficients, between model calculations, and experimental measurements [44–50]. These differences largely arise from the limited understanding of the initial conditions in pp and p-Pb collisions, in particular, the spatial and subnucleonic structure of the proton [43,51–53]. In contrast, in light-ion collisions, such as OO and Ne–Ne, the flow is predicted to be predominantly driven by the shape (eccentricity) of the initial overlap region [54–61]. These geometric features are more precisely characterized when the colliding nuclei have been systematically investigated [62,63]. Even though the ground states of ^{16}O and ^{20}Ne have $J^{\pi} = 0^{+}$, and are therefore spherically symmetric in the laboratory frame, their wave functions can be described as superpositions of intrinsic shapes averaged over all orientations [64]. In modern nuclear-structure models, such intrinsic shapes emerge as a tetrahedral $4-\alpha$ [65] configuration for ^{16}O, while ^{20}Ne resembles an $\alpha + {}^{16}$O"bowling pin"–like structure [66–68] as a consequence of the spatial many-body nucleon correlations. As the even-even $J^{\pi} = 0^{+}$ nuclei are rotationally invariant in the laboratory frame, any mapping of measured flow to ground-state deformations remains inherently model dependent and should be considered complementary to traditional low-energy nuclear-structure constraints [69].

As an example, central heavy-ion collisions were proven to be particularly sensitive to the shape of the nucleus, such as the quadrupole deformation and triaxiality of ^{129}Xe and ^{192}Au nuclei [70–74]. Given that OO and Ne–Ne have similar system sizes [55], the evolution of the two systems is similar, so that the ratios between the two systems substantially mitigate final-state effects (e.g., hadronic rescattering, jet, decay) and thus highlight the differences in the effects of the initial conditions [55,62,63,75], i.e., nuclear shape, subnucleonic structure, and initial fluctuations.

In this Letter, the anisotropic flow measurements are performed utilizing data from the short light-ion runs, and OO and Ne–Ne collisions, delivered by the LHC in July 2025 and recorded with the ALICE apparatus [76]. Similar measurements have been performed at ATLAS around the same time [77] and shortly after by the CMS Collaboration [78]. The centrality of the collisions, which quantifies the fraction of a geometrical cross section of the colliding nuclei, is estimated using the multiplicity measured in the fast interaction trigger detector, located at a pseudorapidity range of $-3.3 < \eta < -2.1$ (FT0C) [76]. Events are required to be within 10 cm of the nominal interaction point. To reject pileup events and optimize the centrality estimation, bunch crossings with more than one reconstructed vertex are rejected. In total, about 3 billion OO collisions and 400 million Ne–Ne collisions pass these criteria.

The charged particles are reconstructed based on information from the inner tracking system (ITS) [76,79] and the time projection chamber (TPC) [80]. High-quality tracks are selected by requiring more than 50 associated TPC clusters, at least 70 crossed rows in the TPC, and five associated ITS clusters, as well as a χ^2 per degree of freedom of the track fit to the TPC space points less than 2.5. Contamination from secondary particles is largely reduced by requiring tracks to have a distance of closest approach (DCA) to the primary vertex of less than 2 cm along the longitudinal direction and a transverse DCA less than a p_{T}-dependent value ranging from 0.2 cm at $p_{\mathrm{T}} = 0.2$ GeV/c to 0.02 cm at $p_{\mathrm{T}} = 3$ GeV/c.

The flow measurements presented in this Letter were obtained from two-particle and multiparticle cumulants using the generic framework [81,82], which corrects for detector acceptance and track reconstruction efficiency effects. To suppress nonflow contamination, which are the azimuthal angle correlations not associated with the nth-order harmonic symmetry plane angle Ψ_{n}, a pseudorapidity separation of $|\Delta\eta| > 1.4$ is applied in the two-particle correlation measurements [83]. The four-particle correlations are, by construction less sensitive to nonflow effects [82]. Thus, the standard method is applied by default, while the subevent method [84] was applied as a cross check.

Systematic uncertainties are estimated with relative differences by varying the event and track selection criteria, and are added to the estimations of the remaining nonflow effects. Uncertainties related to the event selection include the variation in the accepted vertex position along the beam line. The resulting systematic uncertainty was found to be within 2%. In the tracking procedure, the variations of the maximum allowed DCA to the primary vertex, both along the beam line and in the transverse plane, result in differences of less than 1%. To estimate the remaining nonflow contamination, the dihadron correlation method [23,85] with $|\Delta\eta| > 1.4$, together with an additional template fit approach, was examined [26,35]. The deviations from the cumulant measurements are treated as systematic uncertainties associated with nonflow effects. Only the sources of systematic uncertainties found to be statistically significant by more than 1σ following the procedure in Ref. [86] are combined in quadrature to obtain the total systematic uncertainty. As a result, systematic uncertainties up to 6.5% are assigned to $v_n\{2\}$ and $v_2\{4\}$ for both OO and Ne–Ne collisions, and systematic uncertainties within 1.5% are assigned to the ratio $v_n\{2\}(\mathrm{Ne\text{–}Ne/OO})$ and $v_2\{4\}(\mathrm{Ne\text{–}Ne/OO})$.

The centrality dependence of $v_2\{2\}$, $v_3\{2\}$, and $v_2\{4\}$ in OO and Ne–Ne collisions at $\sqrt{s_{\mathrm{NN}}} = 5.36$ TeV is shown in Fig. 1. In both collision systems, $v_2\{2\}$ exhibits a weak centrality dependence; it initially increases with an increasing centrality percentile up to approximately 30%, following the trend of the initial state eccentricity ε_2 [87]. Then, a decrease of the measured $v_2\{2\}$ in more peripheral collisions is observed. The $v_2\{4\}$ measurement also shows an

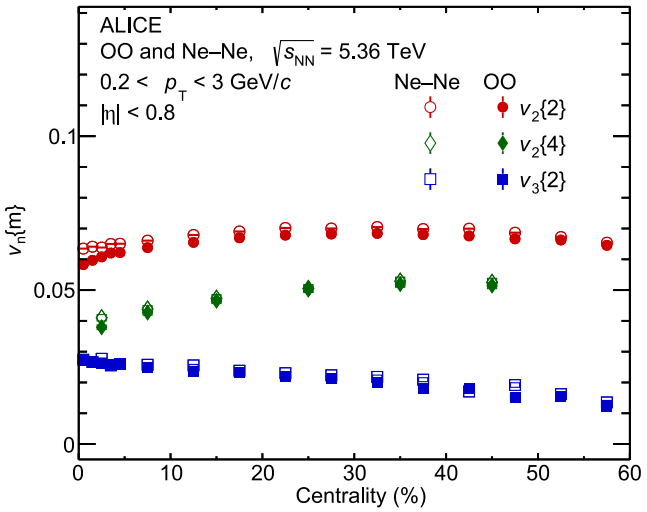


FIG. 1. Charged particle $v_2\{2\}$, $v_3\{2\}$, and $v_2\{4\}$ as a function of centrality in OO (solid markers) and Ne–Ne (open markers) collisions at $\sqrt{s_{NN}} = 5.36$ TeV. The vertical lines represent statistical uncertainties, and the open boxes represent systematic uncertainties, with most of them being smaller than the symbol size.

increasing trend with increasing centrality percentile for the presented centrality region, chosen as the region where the nonflow of $v_2\{4\}$ is under control, and the $v_2\{4\}$ is expected to decrease at higher centralities similar to $v_2\{2\}$. Smaller values of $v_2\{4\}$ compared to $v_2\{2\}$, and the nonzero value of the measured $v_2\{4\}$ indicates the collective nature of the measured anisotropy and confirms the presence of anisotropic flow in OO and Ne–Ne collisions. Assuming that the applied pseudorapidity gap effectively suppresses nonflow effects in two-particle correlations, the remaining differences between two- and four-particle cumulants of v_2 can be attributed to event-by-event fluctuations of elliptic flow, which are further quantified in Fig. 5 in the End Matter. The observed increasing trend of $v_2\{4\}$ with increasing centrality percentile signifies the system's response to the changes of "lenticular" shape formed by the two overlapping nuclei. An increasing trend of $v_2\{4\}$ toward more peripheral collisions (lower multiplicity) was not previously observed in either pp or in p-Pb collisions [11,88], but is observed in Fig. 1 for both OO and Ne–Ne collisions reflecting the geometric initial conditions of these collisions.

In contrast to the v_2 results, $v_3\{2\}$ decreases with larger centrality percentiles. This decreasing trend and the magnitudes of $v_3\{2\}$ are similar to what is seen in the $v_3\{2\}$ measurements in pp and p-Pb collisions [11]. This is expected as $v_3\{2\}$ arises from initial state fluctuations, which are comparable at the same multiplicity in small systems [11,37]. This is also consistent with low-multiplicity measurements of v_3 in Xe–Xe and Pb–Pb collisions [89], confirming the fluctuation-driven nature of v_3 in noncentral collisions across system sizes.

In Fig. 2, the measurements are compared with hydrodynamic simulations from the Trajectum framework [55,87,90], which incorporate nuclear structure inputs for ^{16}O and ^{20}Ne derived from the nuclear lattice effective field theory (NLEFT) [66] and the *ab initio* projected generator

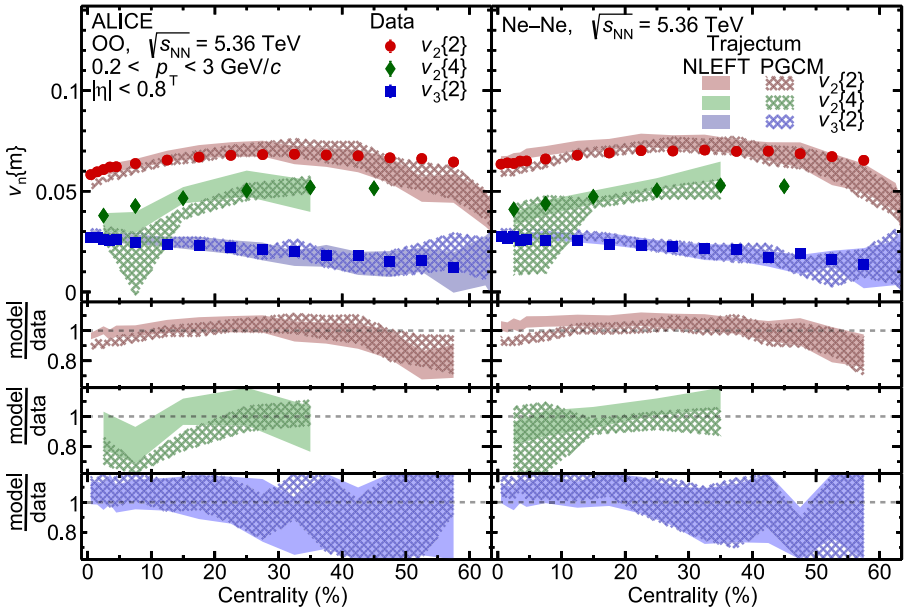


FIG. 2. Charged particle $v_2\{2\}$, $v_3\{2\}$, and $v_2\{4\}$ as a function of centrality in OO (left) and Ne–Ne (right) collisions at $\sqrt{s_{NN}} = 5.36$ TeV. The vertical lines represent statistical uncertainties, and the open boxes represent systematic uncertainties, with most of them being smaller than the symbol size. The measurements are compared with Trajectum calculations with NLEFT and PGCM inputs [55].

coordinate method (PGCM) [67,68]. Both approaches model ground-state nucleon correlations within the nuclei and represent the current best understanding of the nuclear structure. The NLEFT approach constructs nuclear structures from first principles by evolving nucleon configurations via Monte Carlo simulations on a discrete lattice, naturally incorporating many-body correlations and emergent clustering. The PGCM instead starts from energy-minimized mean-field states and includes collective correlations by projecting onto appropriate quantum numbers and mixing configurations across deformation spaces. In both frameworks, as mentioned previously, the ^{20}Ne nuclei exhibit a bowling-pin-like $^{16}\mathrm{O} + \alpha$ structure, while the ^{16}O nuclei have irregular tetrahedronlike shapes [55]. The theoretical predictions are shown as colored curves, with bands indicating the combined statistical and systematic uncertainties. The goal of these comparisons is to assess whether the combination of realistic nuclear structures and a hydrodynamic framework tuned using measurements from heavy-ion collisions can quantitatively predict the experimental measurements in light-ion collisions. As shown in Fig. 2, NLEFT-based calculations successfully reproduce both the trend and magnitude of $v_2\{2\}$, $v_3\{2\}$, and $v_2\{4\}$ up to 50% centrality. The agreements with respect to the flow measurements equal or surpass the accuracy of full Bayesian parameter extraction in previous heavy-ion studies, which have been based on one-body nuclear density distribution of the structure of heavy nuclei (i.e., ^{129}Xe, ^{208}Pb) [18–20]. The agreement between the experimental measurements and theoretical calculations presented in this Letter suggests that developing realistic low-energy *ab initio* calculations for heavier nuclei could significantly improve our understanding of the initial conditions of nuclear collisions, and therefore, enhance the precision of the extraction of QGP properties. In the case of PGCM-based calculations, the agreement is slightly worse in central collisions, though the deviation from the flow measurements remains within a few percentages. In noncentral collisions, the calculations are consistent with the measurements within the uncertainties. In particular, the $v_3\{2\}$ results are highly nontrivial, as the measurements clearly exhibit a different centrality dependence from the initial-state triangular eccentricity ε_3 calculation, which predicts larger values in semicentral than in central collisions [87]. This difference between the initial-state geometric shape and the final-state triangular flow highlights the role of the strong response of the created system, which is accurately captured by the hydrodynamic predictions. It is noteworthy that when centrality is estimated using particle multiplicity in the midrapidity region (which is used in the Trajectum calculations), the $v_2\{2\}$ and $v_3\{2\}$ measurements remain unchanged, while a ~10% reduction in $v_2\{4\}$ is observed, leading to a better agreement with hydrodynamic predictions. The measured $v_2\{4\}$ is accurately described by the hydrodynamic predictions in both OO and Ne–Ne. This is the first time the measurements of a multiparticle cumulant of anisotropic flow can be successfully reproduced by hydrodynamic models in small systems. Notably, the long-standing sign problem present in hydrodynamic descriptions of pp collisions [47,48] is not observed in light-ion collisions. The consistency between the presented $v_2\{2\}$, $v_3\{2\}$, and $v_2\{4\}$ measurements and hydrodynamic model predictions supports the emergence of collective behavior in light-ion collisions, well described by a hydrodynamic expansion of the QGP.

Ratios between two collision systems of comparable size are particularly valuable, as they largely suppress final-state effects and reduce systematic uncertainties for both theoretical model calculations and experimental measurements [91,92]. These ratios serve as sensitive probes of the initial-state geometry and enable rigorous testing of the theoretical understanding of the dynamic evolution in small systems. The centrality dependence of the system-comparison ratios $v_2\{2\}(\mathrm{Ne–Ne/OO})$ and $v_3\{2\}(\mathrm{Ne–Ne/OO})$ is presented in Fig. 3. For $v_2\{2\}(\mathrm{Ne–Ne/OO})$,

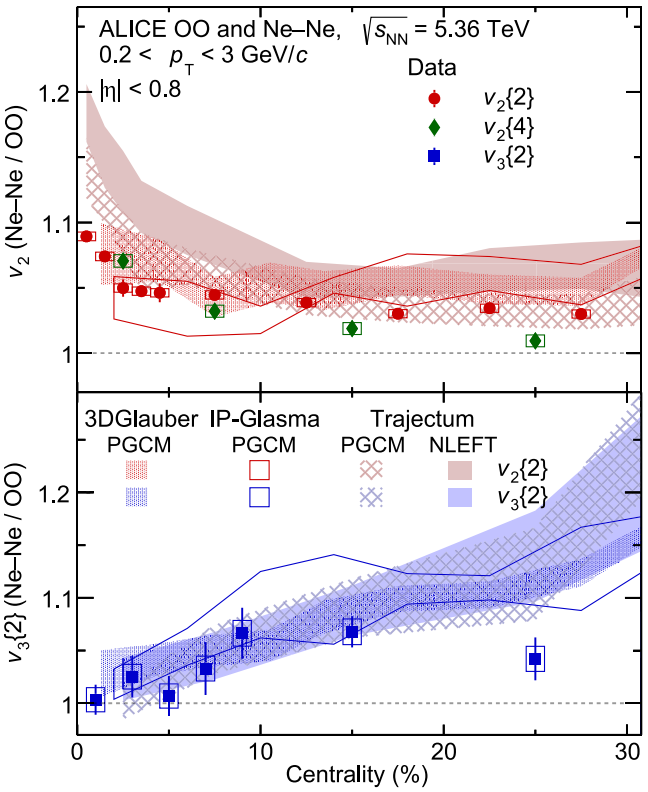


FIG. 3. Ratios $v_2(\mathrm{Ne–Ne/OO})$ and $v_3(\mathrm{Ne–Ne/OO})$ as a function of centrality in the 0%–30% centrality range. The vertical lines represent statistical uncertainties, and the open boxes represent the systematic uncertainties, while most of them are smaller than the symbol size. The measurements are compared with Trajectum calculations with NLEFT and PGCM inputs [55] as well as IP-Glasma + JIMWLK + MUSIC + UrQMD [93] and 3DGlauber + MUSIC + UrQMD [94] calculations with PGCM input.

the ratio peaks at around 1.08 in ultracentral collisions and rapidly decreases to about 1.05 by 10% centrality, after which it exhibits a weak centrality dependence. Similar centrality dependence is also observed in the ratio of $v_2\{4\}(\mathrm{Ne–Ne/OO})$. This pronounced enhancement in central events is attributed to the stronger quadrupole deformation of ^{20}Ne compared to the tetrahedral ^{16}O [55]. In contrast, $v_3\{2\}(\mathrm{Ne–Ne/OO})$ begins around unity in central collisions and increases gradually with increasing centrality percentile, reaching approximately 1.06 at 10%. The smaller $v_3\{2\}$ ratio in central collisions could be attributed to the tetrahedral configuration of ^{16}O, which leads to a larger octupole deformation. This results in a larger triangular eccentricity ε_3 and consequently, a smaller $v_3\{2\}(\mathrm{Ne–Ne/OO})$ in the most central collisions.

As shown in Fig. 2, the measurements of the centrality dependence of anisotropic flow favor the NLEFT-based hydrodynamic calculations. In contrast, the system-comparison ratios are closer to the PGCM-based predictions. Notably, both NLEFT- and PGCM-based hydrodynamic calculations slightly overestimate the measured $v_2\{2\}$ ratios as seen in Fig. 3. Given the fact that the two systems evolve similarly, leading to a suppression of many final-state effects when taking the ratio, this major discrepancy may originate from the modeling of the immediate postcollision initial state. Specifically, parameters governing energy deposition, nucleon and subnucleon spatial profiles, and preequilibrium dynamics may require refinement [63]. It is not known *a priori* whether gluon distributions and saturation in ultrarelativistic collisions affect nuclear structure. Since such effects are not considered in low-energy descriptions but may become important at high energies, the measurements provide a lever for exploring potential differences in nuclear structure across energy scales.

To determine whether the observed discrepancies in the system ratio stem from the initial conditions employed in hydrodynamic calculations or from inaccurate nuclear structure inputs, calculations from both the IP-Glasma + JIMWLK + MUSIC + UrQMD model [93] and the 3DGlauber + MUSIC + UrQMD framework [94] are presented. Both models utilize nuclear structure inputs from *ab initio* PGCM [67,68], identical to those used in the Trajectum predictions. As shown in Fig. 3, the IP-Glasma-based hydrodynamic model describes the system ratios very well, capturing both the trend and the magnitude of the measurements. A comparison to the individual flow coefficients can be found in Fig. 6. The main difference in the system ratio calculations between the Trajectum and IP-Glasma + JIMWLK + MUSIC + UrQMD models most likely lies in their description of the initial conditions immediately after the collisions and early-time dynamics prior to thermalization. The subnucleon width w_q, the effective transverse size over which partons (quarks and gluons) inside a nucleon are distributed, is obtained from Bayesian inference from Pb–Pb collisions and has a size of $w_q \approx 0.40$ fm for the Trajectum model. It is much larger compared to the IP-Glasma + JIMWLK + MUSIC + UrQMD model, which uses a width of $w_q \approx 0.11$ fm inferred from incoherent J/ψ production [95,96] from HERA data [97,98]. At the same time, a reasonable agreement is also seen between the measurements and the 3DGlauber + MUSIC + UrQMD calculations [94], which use a $w_q \approx 0.11$ fm. The determination of the nucleon and subnucleon width with the Bayesian parameter estimation framework has so far proved to be challenging [99], and only recently has the nucleon width been better constrained in Bayesian models [100]. The present measurements favor the calculations with a smaller subnucleon width of approximately 0.1–0.2 fm, as previously suggested [63]. Although other processes or assumptions of the initial-state models may contribute to the differences, such measurements provide additional constraints for improving the description of the early-time structure and dynamics of the QGP, and the inclusion of the ratio measurements in future Bayesian analyses will allow for a more precise extraction of the subnucleon width of the light nuclei.

This Letter presents the first measurements of elliptic flow (v_2) and triangular flow (v_3) in OO and Ne–Ne collisions at $\sqrt{s_{\mathrm{NN}}} = 5.36$ TeV using the ALICE detector. The flow coefficients exhibit characteristic centrality dependence in both collision systems, which was not observed previously in pp and p-Pb collisions. The combination of nuclear structure inputs from the NLEFT and PGCM model together with the standard modeling framework of relativistic heavy-ion collisions, the hydrodynamic model, shows a reasonable agreement with the anisotropic flow measurements in a wide range of centralities. Importantly, the NLEFT and PGCM models utilise the many-body nuclear densities to determine the distribution of nucleons [55] as emphasised in Ref. [69]. The agreement between theoretical predictions and experimental measurements reported in this Letter reveals the emergence of hydrodynamic flow across collision systems at the LHC, effectively bridging the gap between heavy-ion collisions and proton-proton and proton-nucleus collisions. Moreover, the ratios between OO and Ne–Ne collisions substantially reduce the influence from the final-state effects and serve as precise probes of the initial conditions. The pronounced enhancement of $v_2\{2\}(\mathrm{Ne–Ne/OO})$ observed in central collisions is attributed to the significant nuclear geometric effects of ^{16}O and ^{20}Ne nuclei on the final-state flow coefficients. The comparison of the measured $v_2\{2\}(\mathrm{Ne–Ne/OO})$ with the various hydrodynamic model calculations, including state of the art nuclear structure, points to imperfect configurations of the initial conditions, particularly the subnucleon size. These precision measurements, therefore, offer a unique probe into the early-time dynamics and (sub)structure of the colliding nuclei. They open new avenues for imaging the nuclear

structure of light ions in the near future, complementary to low-energy nuclear-structure experiments such as the α-cluster configurations in ^{16}O and ^{20}Ne, which have profound implications for understanding quantum many-body phenomena, a longstanding challenge in nuclear physics.

Acknowledgments—The ALICE Collaboration would like to thank Giuliano Giacalone, Govert Nijs, Wilke van der Schee (Trajectum), Chun Shen, Bjoern Schenke, Wenbin Zhao (IP-Glasma + MUSIC + UrQMD), Chun Shen, Wenbin Zhao (3D-Glauber+MUSIC + UrQMD), Ziwei Lin, Guoliang Ma, and Xinli Zhao (AMPT) for providing the latest predictions. The ALICE Collaboration would like to thank all its engineers and technicians for their invaluable contributions to the construction of the experiment and the CERN accelerator teams for the outstanding performance of the LHC complex. The ALICE Collaboration gratefully acknowledges the resources and support provided by all Grid centers and the Worldwide LHC Computing Grid (WLCG) Collaboration. The ALICE Collaboration acknowledges the following funding agencies for their support in building and running the ALICE detector: A. I. Alikhanyan National Science Laboratory (Yerevan Physics Institute) Foundation (ANSL), State Committee of Science and World Federation of Scientists (WFS), Armenia; Austrian Academy of Sciences, Austrian Science Fund (FWF): [M 2467-N36] and Nationalstiftung für Forschung, Technologie und Entwicklung, Austria; Ministry of Communications and High Technologies, National Nuclear Research Center, Azerbaijan; Rede Nacional de Física de Altas Energias (Renafae), Financiadora de Estudos e Projetos (Finep), Fundação de Amparo à Pesquisa do Estado de São Paulo (FAPESP) and The Sao Paulo Research Foundation (FAPESP), Brazil; Bulgarian Ministry of Education and Science, within the National Roadmap for Research Infrastructures 2020-2027 (object CERN), Bulgaria; Ministry of Education of China (MOEC), Ministry of Science & Technology of China (MSTC) and National Natural Science Foundation of China (NSFC), China; Ministry of Science and Education and Croatian Science Foundation, Croatia; Centro de Aplicaciones Tecnológicas y Desarrollo Nuclear (CEADEN), Cubaenergía, Cuba; Ministry of Education, Youth and Sports of the Czech Republic, Czech Republic; The Danish Council for Independent Research | Natural Sciences, the VILLUM FONDEN and Danish National Research Foundation (DNRF), Denmark; Helsinki Institute of Physics (HIP), Finland; Commissariat à l'Energie Atomique (CEA) and Institut National de Physique Nucléaire et de Physique des Particules (IN2P3) and Centre National de la Recherche Scientifique (CNRS), France; Bundesministerium für Forschung, Technologie und Raumfahrt (BMFTR) and GSI Helmholtzzentrum für Schwerionenforschung GmbH, Germany; General Secretariat for Research and Technology, Ministry of Education, Research and Religions, Greece; National Research, Development and Innovation Office, Hungary; Department of Atomic Energy Government of India (DAE), Department of Science and Technology, Government of India (DST), University Grants Commission, Government of India (UGC) and Council of Scientific and Industrial Research (CSIR), India; National Research and Innovation Agency—BRIN, Indonesia; Istituto Nazionale di Fisica Nucleare (INFN), Italy; Japanese Ministry of Education, Culture, Sports, Science and Technology (MEXT) and Japan Society for the Promotion of Science (JSPS) KAKENHI, Japan; Consejo Nacional de Ciencia (CONACYT) y Tecnología, through Fondo de Cooperación Internacional en Ciencia y Tecnología (FONCICYT) and Dirección General de Asuntos del Personal Academico (DGAPA), Mexico; Nederlandse Organisatie voor Wetenschappelijk Onderzoek (NWO), Netherlands; The Research Council of Norway, Norway; Pontificia Universidad Católica del Perú, Peru; Ministry of Science and Higher Education, National Science Centre and WUT ID-UB, Poland; Korea Institute of Science and Technology Information and National Research Foundation of Korea (NRF), Republic of Korea; Ministry of Education and Scientific Research, Institute of Atomic Physics, Ministry of Research and Innovation and Institute of Atomic Physics and Universitatea Nationala de Stiinta si Tehnologie Politehnica Bucuresti, Romania; Ministerstvo skolstva, vyskumu, vyvoja a mladeze SR, Slovakia; National Research Foundation of South Africa, South Africa; Swedish Research Council (VR) and Knut & Alice Wallenberg Foundation (KAW), Sweden; European Organization for Nuclear Research, Switzerland; Suranaree University of Technology (SUT), National Science and Technology Development Agency (NSTDA) and National Science, Research and Innovation Fund (NSRF via PMU-B B05F650021), Thailand; Turkish Energy, Nuclear and Mineral Research Agency (TENMAK), Turkey; National Academy of Sciences of Ukraine, Ukraine; Science and Technology Facilities Council (STFC), United Kingdom; and National Science Foundation of the United States of America (NSF) and United States Department of Energy, Office of Nuclear Physics (DOE NP), United States of America. In addition, individual groups or members have received support from the following: Czech Science Foundation (Grant No. 23-07499S), Czech Republic; FORTE project, Reg. No. CZ.02.01.01/00/22_008/0004632, Czech Republic, cofunded by the European Union, Czech Republic; European Research Council (Grant No. 950692), European Union; Deutsche Forschungs Gemeinschaft (DFG, German Research Foundation) "Neutrinos and Dark Matter in Astro- and Particle Physics" (Grant No. SFB 1258), Germany; CONVECS project, CUP C97H23001700002 FESR

2021-2027 program, Italy; and FAIR—Future Artificial Intelligence Research, funded by the NextGenerationEU program (Italy).

Data availability—The data that support the findings of this article are openly available [101].

[1] J. Adams *et al.* (STAR Collaboration), Experimental and theoretical challenges in the search for the quark gluon plasma: The STAR Collaboration's critical assessment of the evidence from RHIC collisions, Nucl. Phys. **A757**, 102 (2005).

[2] K. Adcox *et al.* (PHENIX Collaboration), Formation of dense partonic matter in relativistic nucleus-nucleus collisions at RHIC: Experimental evaluation by the PHENIX Collaboration, Nucl. Phys. **A757**, 184 (2005).

[3] B. B. Back *et al.* (PHOBOS Collaboration), The PHOBOS perspective on discoveries at RHIC, Nucl. Phys. **A757**, 28 (2005).

[4] S. Acharya *et al.* (ALICE Collaboration), The ALICE experiment: A journey through QCD, Eur. Phys. J. C **84**, 813 (2024).

[5] A. Hayrapetyan *et al.* (CMS Collaboration), Overview of high-density QCD studies with the CMS experiment at the LHC, Phys. Rep. **1115**, 219 (2025).

[6] J.-Y. Ollitrault, Anisotropy as a signature of transverse collective flow, Phys. Rev. D **46**, 229 (1992).

[7] K. Aamodt *et al.* (ALICE Collaboration), Higher harmonic anisotropic flow measurements of charged particles in Pb–Pb collisions at $\sqrt{s_{\rm NN}} = 2.76$ TeV, Phys. Rev. Lett. **107**, 032301 (2011).

[8] B. Abelev *et al.* (ALICE Collaboration), Elliptic flow of identified hadrons in Pb-Pb collisions at $\sqrt{s_{\rm NN}} =$ 2.76 TeV, J. High Energy Phys. 06 (2015) 190.

[9] J. Adam *et al.* (ALICE Collaboration), Anisotropic flow of charged particles in Pb-Pb collisions at $\sqrt{s_{\rm NN}} = 5.02$ TeV, Phys. Rev. Lett. **116**, 132302 (2016).

[10] S. Acharya *et al.* (ALICE Collaboration), Anisotropic flow in Xe-Xe collisions at $\sqrt{s_{\rm NN}} = 5.44$ TeV, Phys. Lett. B **784**, 82 (2018).

[11] S. Acharya *et al.* (ALICE Collaboration), Investigations of anisotropic flow using multiparticle azimuthal correlations in pp, p-Pb, Xe-Xe, and Pb-Pb collisions at the LHC, Phys. Rev. Lett. **123**, 142301 (2019).

[12] S. Acharya *et al.* (ALICE Collaboration), Anisotropic flow and flow fluctuations of identified hadrons in Pb–Pb collisions at $\sqrt{s_{\rm NN}} = 5.02$ TeV, J. High Energy Phys. 05 (2023) 243.

[13] G. Aad *et al.* (ATLAS Collaboration), Measurement of the azimuthal anisotropy for charged particle production in $\sqrt{s_{\rm NN}} = 2.76$ TeV lead-lead collisions with the ATLAS detector, Phys. Rev. C **86**, 014907 (2012).

[14] G. Aad *et al.* (ATLAS Collaboration), Measurement of the azimuthal anisotropy of charged-particle production in Xe–Xe collisions at $\sqrt{s_{\rm NN}} = 5.44$ TeV with the ATLAS detector, Phys. Rev. C **101**, 024906 (2020).

[15] S. Chatrchyan *et al.* (CMS Collaboration), Measurement of higher-order harmonic azimuthal anisotropy in Pb–Pb collisions at $\sqrt{s_{\rm NN}} = 2.76$ TeV, Phys. Rev. C **89**, 044906 (2014).

[16] A. M. Sirunyan *et al.* (CMS Collaboration), Charged-particle angular correlations in Xe–Xe collisions at $\sqrt{s_{\rm NN}} = 5.44$ TeV, Phys. Rev. C **100**, 044902 (2019).

[17] U. Heinz and R. Snellings, Collective flow and viscosity in relativistic heavy-ion collisions, Annu. Rev. Nucl. Part. Sci. **63**, 123 (2013).

[18] J. E. Bernhard, J. S. Moreland, S. A. Bass, J. Liu, and U. Heinz, Applying Bayesian parameter estimation to relativistic heavy-ion collisions: Simultaneous characterization of the initial state and quark-gluon plasma medium, Phys. Rev. C **94**, 024907 (2016).

[19] D. Everett *et al.* (JETSCAPE Collaboration), Phenomenological constraints on the transport properties of QCD matter with data-driven model averaging, Phys. Rev. Lett. **126**, 242301 (2021).

[20] G. Nijs, W. van der Schee, U. Gürsoy, and R. Snellings, Transverse momentum differential global analysis of heavy-ion collisions, Phys. Rev. Lett. **126**, 202301 (2021).

[21] P. Kovtun, D. T. Son, and A. O. Starinets, Viscosity in strongly interacting quantum field theories from black hole physics, Phys. Rev. Lett. **94**, 111601 (2005).

[22] Z. Citron *et al.*, Report from working group 5: Future physics opportunities for high-density QCD at the LHC with heavy-ion and proton beams, CERN Yellow Rep. Monogr. **7**, 1159 (2019).

[23] V. Khachatryan *et al.* (CMS Collaboration), Observation of long-range near-side angular correlations in proton-proton collisions at the LHC, J. High Energy Phys. 09 (2010) 091.

[24] B. Abelev *et al.* (ALICE Collaboration), Long-range angular correlations of π, K and p in p-Pb collisions at $\sqrt{s_{\rm NN}} = 5.02$ TeV, Phys. Lett. B **726**, 164 (2013).

[25] V. Khachatryan *et al.* (CMS Collaboration), Long-range two-particle correlations of strange hadrons with charged particles in pPb and Pb–Pb collisions at LHC energies, Phys. Lett. B **742**, 200 (2015).

[26] G. Aad *et al.* (ATLAS Collaboration), Observation of long-range elliptic azimuthal anisotropies in $\sqrt{s} = 13$ and 2.76 TeV pp collisions with the ATLAS detector, Phys. Rev. Lett. **116**, 172301 (2016).

[27] PHENIX Collaboration, Creation of quark–gluon plasma droplets with three distinct geometries, Nat. Phys. **15**, 214 (2019).

[28] A. M. Sirunyan *et al.* (CMS Collaboration), Elliptic flow of charm and strange hadrons in high-multiplicity pPb collisions at $\sqrt{s_{\rm NN}} = 8.16$ TeV, Phys. Rev. Lett. **121**, 082301 (2018).

[29] S. Acharya *et al.* (ALICE Collaboration), Measurements of long-range two-particle correlation over a wide pseudorapidity range in p–Pb collisions at $\sqrt{s_{\rm NN}} = 5.02$ TeV, J. High Energy Phys. 01 (**2024**) 199.

[30] S. Acharya *et al.* (ALICE Collaboration), First observation of ultra-long-range azimuthal correlations in low multiplicity pp and p-Pb collisions at the LHC, arXiv:2504.02359.

[31] L. Adamczyk *et al.* (STAR Collaboration), Long-range pseudorapidity dihadron correlations in $d+$Au collisions at $\sqrt{s_{\rm NN}} = 200$ GeV, Phys. Lett. B **747**, 265 (2015).

[32] A. Adare *et al.* (PHENIX Collaboration), Measurement of long-range angular correlation and quadrupole anisotropy of pions and (anti)protons in central $d+\mathrm{Au}$ collisions at $\sqrt{s_{NN}}=200$ GeV, Phys. Rev. Lett. **114**, 192301 (2015).

[33] Y.-C. Chen *et al.* (Electron-Positron Alliance Collaboration), Long-range near-side correlation in e^+e^- collisions at 183–209 GeV with ALEPH archived data, Phys. Lett. B **856**, 138957 (2024).

[34] M. I. Abdulhamid *et al.* (STAR Collaboration), Measurements of the elliptic and triangular azimuthal anisotropies in central $\mathrm{He3}+\mathrm{Au}$, $\mathrm{d}+\mathrm{Au}$ and $\mathrm{p}+\mathrm{Au}$ collisions at $\sqrt{s_{\mathrm{NN}}}=200$ GeV, Phys. Rev. Lett. **130**, 242301 (2023).

[35] S. Acharya *et al.* (ALICE Collaboration), Observation of partonic flow in proton-proton and proton-nucleus collisions, Nat. Commun. **17**, 2585 (2026).

[36] V. Khachatryan *et al.* (CMS Collaboration), Evidence for collective multiparticle correlations in p-Pb collisions, Phys. Rev. Lett. **115**, 012301 (2015).

[37] V. Khachatryan *et al.* (CMS Collaboration), Evidence for collectivity in pp collisions at the LHC, Phys. Lett. B **765**, 193 (2017).

[38] M. Aaboud *et al.* (ATLAS Collaboration), Measurement of long-range multiparticle azimuthal correlations with the subevent cumulant method in pp and p–Pb collisions with the ATLAS detector at the CERN Large Hadron Collider, Phys. Rev. C **97**, 024904 (2018).

[39] H. Song, Y. Zhou, and K. Gajdosova, Collective flow and hydrodynamics in large and small systems at the LHC, Nucl. Sci. Tech. **28**, 99 (2017).

[40] J. L. Nagle and W. A. Zajc, Small system collectivity in relativistic hadronic and nuclear collisions, Annu. Rev. Nucl. Part. Sci. **68**, 211 (2018).

[41] P. Christiansen and P. Van Mechelen, Soft QCD physics at the LHC: Highlights and opportunities, Annu. Rev. Nucl. Part. Sci. **75**, 327 (2025).

[42] J. F. Grosse-Oetringhaus and U. A. Wiedemann, A decade of collectivity in small systems, Report No. CERN-TH-2024-110, arXiv:2407.07484.

[43] W. Zhao, C. M. Ko, Y.-X. Liu, G.-Y. Qin, and H. Song, Probing the partonic degrees of freedom in high-multiplicity p–Pb collisions at $\sqrt{s_{\mathrm{NN}}}=5.02$ TeV, Phys. Rev. Lett. **125**, 072301 (2020).

[44] P. Bozek, Collective flow in p-Pb and d-Pb collisions at TeV energies, Phys. Rev. C **85**, 014911 (2012).

[45] H. Mäntysaari, B. Schenke, C. Shen, and P. Tribedy, Imprints of fluctuating proton shapes on flow in proton-lead collisions at the LHC, Phys. Lett. B **772**, 681 (2017).

[46] R. D. Weller and P. Romatschke, One fluid to rule them all: viscous hydrodynamic description of event-by-event central $\mathrm{p}+\mathrm{p}$, $\mathrm{p}+\mathrm{Pb}$ and $\mathrm{Pb}+\mathrm{Pb}$ collisions at $\sqrt{s}=5.02$ TeV, Phys. Lett. B **774**, 351 (2017).

[47] W. Zhao, Y. Zhou, H. Xu, W. Deng, and H. Song, Hydrodynamic collectivity in proton–proton collisions at 13 TeV, Phys. Lett. B **780**, 495 (2018).

[48] W. Zhao, Y. Zhou, K. Murase, and H. Song, Searching for small droplets of hydrodynamic fluid in proton–proton collisions at the LHC, Eur. Phys. J. C **80**, 846 (2020).

[49] L. He, T. Edmonds, Z.-W. Lin, F. Liu, D. Molnar, and F. Wang, Anisotropic parton escape is the dominant source of azimuthal anisotropy in transport models, Phys. Lett. B **753**, 506 (2016).

[50] A. Kurkela, U. A. Wiedemann, and B. Wu, Nearly isentropic flow at sizeable η/s, Phys. Lett. B **783**, 274 (2018).

[51] Y. Wang, W. Zhao, and H. Song, Exploring the partonic collectivity in small systems at the LHC, Phys. Rev. C **113**, 024901 (2026).

[52] B. Schenke, C. Shen, and P. Tribedy, Running the gamut of high energy nuclear collisions, Phys. Rev. C **102**, 044905 (2020).

[53] H. Mäntysaari, B. Schenke, C. Shen, and W. Zhao, Bayesian inference of the fluctuating proton shape, Phys. Lett. B **833**, 137348 (2022).

[54] S. Zhang, Y. G. Ma, J. H. Chen, W. B. He, and C. Zhong, Nuclear cluster structure effect on elliptic and triangular flows in heavy-ion collisions, Phys. Rev. C **95**, 064904 (2017).

[55] G. Giacalone *et al.*, Exploiting ^{20}Ne isotopes for precision characterizations of collectivity in small systems, Phys. Rev. Lett. **135**, 012302 (2025).

[56] Y.-A. Li, S. Zhang, and Y.-G. Ma, Signatures of α-clustering in ^{16}O by using a multiphase transport model, Phys. Rev. C **102**, 054907 (2020).

[57] Y. Wang, S. Zhao, B. Cao, H.-j. Xu, and H. Song, Exploring the compactness of α clusters in ^{16}O nuclei with relativistic $^{16}O+{}^{16}O$ collisions, Phys. Rev. C **109**, L051904 (2024).

[58] X.-L. Zhao, G.-L. Ma, Y. Zhou, Z.-W. Lin, and C. Zhang, Nuclear cluster structure effect in $^{16}\mathrm{O}+{}^{16}\mathrm{O}$ collisions at the top RHIC energy, Phys. Lett. B **874**, 140254 (2026).

[59] S. H. Lim, J. Carlson, C. Loizides, D. Lonardoni, J. E. Lynn, J. L. Nagle, J. D. Orjuela Koop, and J. Ouellette, Exploring new small system geometries in heavy ion collisions, Phys. Rev. C **99**, 044904 (2019).

[60] N. Summerfield, B.-N. Lu, C. Plumberg, D. Lee, J. Noronha-Hostler, and A. Timmins, ^{16}O ^{16}O collisions at energies available at the BNL relativistic heavy ion collider and at the CERN Large Hadron Collider comparing α clustering versus substructure, Phys. Rev. C **104**, L041901 (2021).

[61] D. Behera, S. Prasad, N. Mallick, and R. Sahoo, Effects of clustered nuclear geometry on the anisotropic flow in O-O collisions at the LHC within a multiphase transport model framework, Phys. Rev. D **108**, 054022 (2023).

[62] J. Jia *et al.*, Imaging the initial condition of heavy-ion collisions and nuclear structure across the nuclide chart, Nucl. Sci. Techn. **35**, 220 (2024).

[63] G. Giacalone *et al.*, Nuclear physics confronts relativistic collisions of isobars, Report of the EMMI RRTF, arXiv:2507.01454.

[64] P. Ring and P. Schuck, *The Nuclear Many-Body Problem* (Springer, Heidelberg, 1980).

[65] An α particle is a tightly bound state of two protons and two neutrons.

[66] D. Lee, Lattice effective field theory simulations of nuclei, Annu. Rev. Nucl. Part. Sci. **75**, 109 (2025).

[67] M. Frosini, T. Duguet, J.-P. Ebran, and V. Somà, Multi-reference many-body perturbation theory for nuclei: I. Novel PGCM-PT formalism, Eur. Phys. J. A **58**, 62 (2022).

[68] M. Frosini, T. Duguet, J.-P. Ebran, B. Bally, T. Mongelli, T. R. Rodríguez, R. Roth, and V. Somà, Multi-reference many-body perturbation theory for nuclei: II. *Ab initio* study of neon isotopes via PGCM and IM-NCSM calculations, Eur. Phys. J. A **58**, 63 (2022).

[69] J. Dobaczewski, A. Gade, K. Godbey, R. V. F. Janssens, and W. Nazarewicz, Extraction of ground-state nuclear deformations from ultrarelativistic heavy-ion collisions: Nuclear structure physics context, Phys. Rev. Res. **7**, 043159 (2025).

[70] L. Adamczyk *et al.* (STAR Collaboration), Azimuthal anisotropy in U + U and Au + Au collisions at RHIC, Phys. Rev. Lett. **115**, 222301 (2015).

[71] M. I. Abdulhamid *et al.* (STAR Collaboration), Imaging shapes of atomic nuclei in high-energy nuclear collisions, Nature (London) **635**, 67 (2024).

[72] S. Acharya *et al.* (ALICE Collaboration), Characterizing the initial conditions of heavy-ion collisions at the LHC with mean transverse momentum and anisotropic flow correlations, Phys. Lett. B **834**, 137393 (2022).

[73] G. Aad *et al.* (ATLAS Collaboration), Correlations between flow and transverse momentum in Xe + Xe and Pb + Pb collisions at the LHC with the ATLAS detector: A probe of the heavy-ion initial state and nuclear deformation, Phys. Rev. C **107**, 054910 (2023).

[74] ALICE Collaboration, Exploring nuclear structure with multiparticle azimuthal correlations at the LHC, Phys. Lett. B **869**, 139855 (2025).

[75] S. Zhang, Y. G. Ma, G. L. Ma, J. H. Chen, Q. Y. Shou, W. B. He, and C. Zhong, Collision system size scan of collective flows in relativistic heavy-ion collisions, Phys. Lett. B **804**, 135366 (2020).

[76] S. Acharya *et al.* (ALICE Collaboration), ALICE upgrades during the LHC long shutdown 2, J. Instrum. **19**, P05062 (2024).

[77] G. Aad *et al.* (ATLAS Collaboration), Measurement of the azimuthal anisotropy of charged particles in $\sqrt{s_{\mathrm{NN}}} =$ 5.36 TeV ^{16}O + ^{16}O and ^{20}Ne + ^{20}Ne collisions with the ATLAS detector, Phys. Rev. C **113**, 045205 (2026).

[78] A. Hayrapetyan *et al.* (CMS Collaboration), following Letter, Observation of long-range collective flow in O + O and Ne + Ne collisions and implications for nuclear structure studies, Phys. Rev. Lett. **137**, 082302 (2026).

[79] B. Abelev *et al.* (ALICE Collaboration), Technical design report for the upgrade of the ALICE inner tracking system, J. Phys. G **41**, 087002 (2014).

[80] J. Adolfsson *et al.* (ALICE TPC Collaboration), The upgrade of the ALICE TPC with GEMs and continuous readout, J. Instrum. **16**, P03022 (2021).

[81] A. Bilandzic, C. H. Christensen, K. Gulbrandsen, A. Hansen, and Y. Zhou, Generic framework for anisotropic flow analyses with multiparticle azimuthal correlations, Phys. Rev. C **89**, 064904 (2014).

[82] Z. Moravcova, K. Gulbrandsen, and Y. Zhou, Generic algorithm for multiparticle cumulants of azimuthal correlations in high energy nucleus collisions, Phys. Rev. C **103**, 024913 (2021).

[83] Y. Zhou, X. Zhu, P. Li, and H. Song, Investigation of possible hadronic flow in $\sqrt{s_{\mathrm{NN}}} = 5.02$ TeV p–Pb collisions, Phys. Rev. C **91**, 064908 (2015).

[84] P. Huo, K. Gajdosov, J. Jia, and Y. Zhou, Importance of non-flow in mixed-harmonic multi-particle correlations in small collision systems, Phys. Lett. B **777**, 201 (2018).

[85] B. Abelev *et al.* (ALICE Collaboration), Long-range angular correlations on the near and away side in p–Pb collisions at $\sqrt{s_{\mathrm{NN}}} = 5.02$ TeV, Phys. Lett. B **719**, 29 (2013).

[86] R. Barlow, Systematic errors: Facts and fictions, *in Conference on Advanced Statistical Techniques in Particle Physics* (2002), pp. 134–144, arXiv:hep-ex/0207026.

[87] G. Nijs and W. van der Schee, Predictions and postdictions for relativistic lead and oxygen collisions with the computational simulation code Trajectum, Phys. Rev. C **106**, 044903 (2022).

[88] S. Chatrchyan *et al.* (CMS Collaboration), Multiplicity and transverse momentum dependence of two- and four-particle correlations in pPb and Pb–Pb collisions, Phys. Lett. B **724**, 213 (2013).

[89] M. Aaboud *et al.* (ATLAS Collaboration), Measurement of long-range multiparticle azimuthal correlations with the subevent cumulant method in pp and p–Pb collisions with the ATLAS detector at the CERN Large Hadron Collider, Phys. Rev. C **97**, 024904 (2018).

[90] G. Nijs, W. van der Schee, U. Gürsoy, and R. Snellings, Bayesian analysis of heavy ion collisions with the heavy ion computational framework Trajectum, Phys. Rev. C **103**, 054909 (2021).

[91] G. Giacalone, J. Jia, and V. Somà, Accessing the shape of atomic nuclei with relativistic collisions of isobars, Phys. Rev. C **104**, L041903 (2021).

[92] M. Abdallah *et al.* (STAR Collaboration), Search for the chiral magnetic effect with isobar collisions at $\sqrt{s_{\mathrm{NN}}} = 200$ GeV by the STAR Collaboration at the BNL relativistic heavy ion collider, Phys. Rev. C **105**, 014901 (2022).

[93] H. Mäntysaari, B. Schenke, C. Shen, and W. Zhao, Collision-energy dependence in heavy-ion collisions from nonlinear QCD evolution, Phys. Rev. Lett. **135**, 022302 (2025).

[94] S. A. Jahan, H. Roch, and C. Shen, Bayesian analysis of (3 + 1)D relativistic nuclear dynamics with the RHIC beam energy scan data, Phys. Rev. C **110**, 054905 (2024).

[95] H. Mäntysaari and B. Schenke, Evidence of strong proton shape fluctuations from incoherent diffraction, Phys. Rev. Lett. **117**, 052301 (2016).

[96] H. Mäntysaari and B. Schenke, Revealing proton shape fluctuations with incoherent diffraction at high energy, Phys. Rev. D **94**, 034042 (2016).

[97] A. Caldwell and H. Kowalski, Investigating the gluonic structure of nuclei via J/ψ scattering, Phys. Rev. C **81**, 025203 (2010).

[98] B. Schenke, P. Tribedy, and R. Venugopalan, Event-by-event gluon multiplicity, energy density, and eccentricities in ultrarelativistic heavy-ion collisions, Phys. Rev. C **86**, 034908 (2012).

[99] G. Giacalone, B. Schenke, and C. Shen, Constraining the nucleon size with relativistic nuclear collisions, Phys. Rev. Lett. **128**, 042301 (2022).

[100] H. Mäntysaari, H. Roch, F. Salazar, B. Schenke, C. Shen, and W. Zhao, Global Bayesian analysis of J/ψ photoproduction on proton and lead targets, Phys. Rev. D **113**, 014038 (2026).

[101] ALICE Collaboration, Evidence of nuclear geometry-driven anisotropic flow in OO and Ne–Ne collisions at $\sqrt{s_{\rm NN}} = 5.36$ TeV, HEPData (Collection) (2026), https://www.hepdata.net/record/ins2967353.

[102] X. Chen, X.-Y. Wu, S. Cao, and G.-Y. Qin, System-size and shape dependencies of collective-flow fluctuations in relativistic nuclear collisions, Phys. Rev. C **109**, 064915 (2024).

[103] C. Zhang, J. Chen, G. Giacalone, S. Huang, J. Jia, and Y.-G. Ma, Ab-initio nucleon-nucleon correlations and their impact on high energy ^{16}O + ^{16}O collisions, Phys. Lett. B **862**, 139322 (2025).

End Matter

This section presents the ratios of $v_3\{2\}/v_2\{2\}$ and $v_2\{4\}/v_2\{2\}$, together with the double ratios comparing both collision systems. The predicted shapes for ^{16}O and ^{20}Ne nuclei have different quadrupole and octupole deformations. In other words, ^{16}O has stronger octupole deformation because of its tetrahedral shape, whereas ^{20}Ne has stronger quadrupole deformation because of its "bowling-pin"-like shape. Therefore, the ratio of $v_3\{2\}/v_2\{2\}$ in OO collisions is expected to be larger than that in Ne–Ne collisions. As shown in Fig. 4, this expectation is confirmed only in the most central collisions, where the nuclear geometric effect is strongest. Beyond this region, the ratio of $v_3\{2\}/v_2\{2\}$ shown in the top panel exhibits a decreasing trend with increasing centrality in both collision systems, with the ratio in OO collisions remaining slightly higher than in Ne–Ne collisions in the most central collisions. Both NLEFT- and PGCM-based hydrodynamic calculations describe the measurements, demonstrating the impact of the unique nuclear shape imprinted by the α-cluster structures in ^{16}O and ^{20}Ne.

In the hydrodynamic evolution picture, elliptic flow arises from the anisotropic expansion of the QGP, which is driven by the spatial distribution of nucleons in the colliding nuclei. The v_2 from two- and four-particle cumulants carries different sensitivities to the event-by-event flow fluctuations, originating from the initial geometry fluctuations. The ratio of $v_2\{4\}/v_2\{2\}$ minimizes the

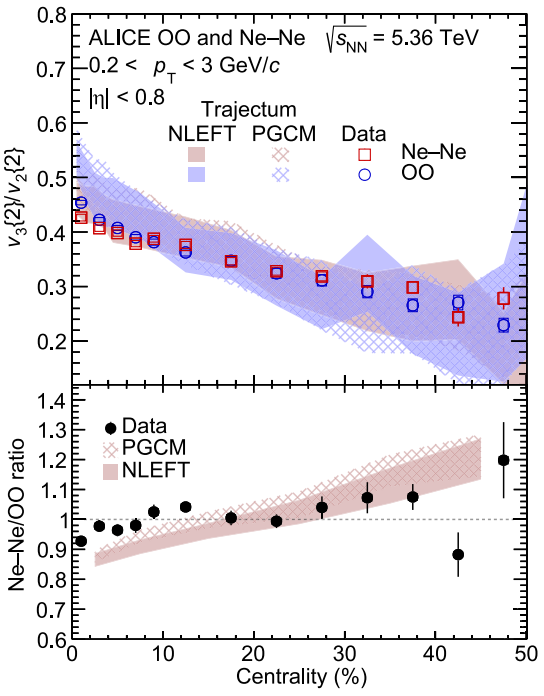


FIG. 4. Top: ratio of the charged particle $v_3\{2\}$ to $v_2\{2\}$ as a function of centrality in OO and Ne–Ne collisions at $\sqrt{s_{\rm NN}} = 5.36$ TeV. Bottom: double ratios $v_3\{2\}/v_2\{2\}$(Ne–Ne:OO). The vertical lines represent statistical uncertainties, and the open boxes represent the systematic uncertainties while most of them are smaller than the symbol size. The measurements are compared with Trajectum calculations with NLEFT and PGCM inputs [55].

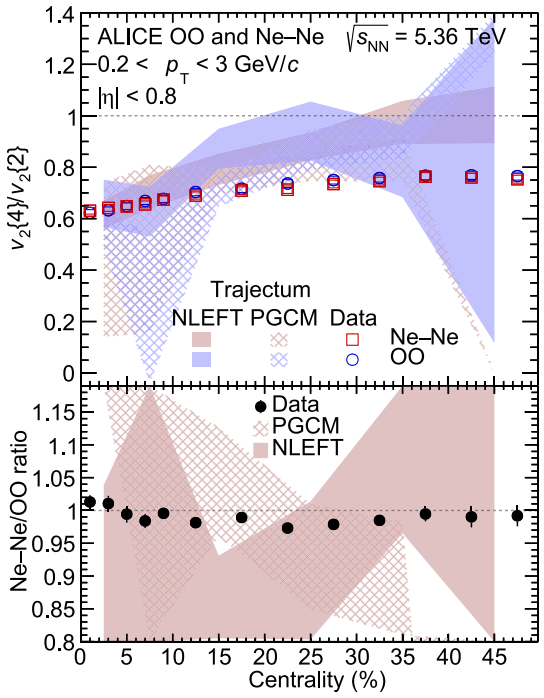


FIG. 5. Top: ratio of the charged particle $v_2\{4\}$ to $v_2\{2\}$ as a function of centrality in OO and Ne–Ne collisions at $\sqrt{s_{\rm NN}} = 5.36$ TeV. Bottom: double ratios $v_2\{4\}/v_2\{2\}$(Ne–Ne:OO). The vertical lines represent statistical uncertainties, and the open boxes represent the systematic uncertainties while most of them are smaller than symbol size. The measurements are compared to Trajectum calculations with NLEFT and PGCM inputs [55].

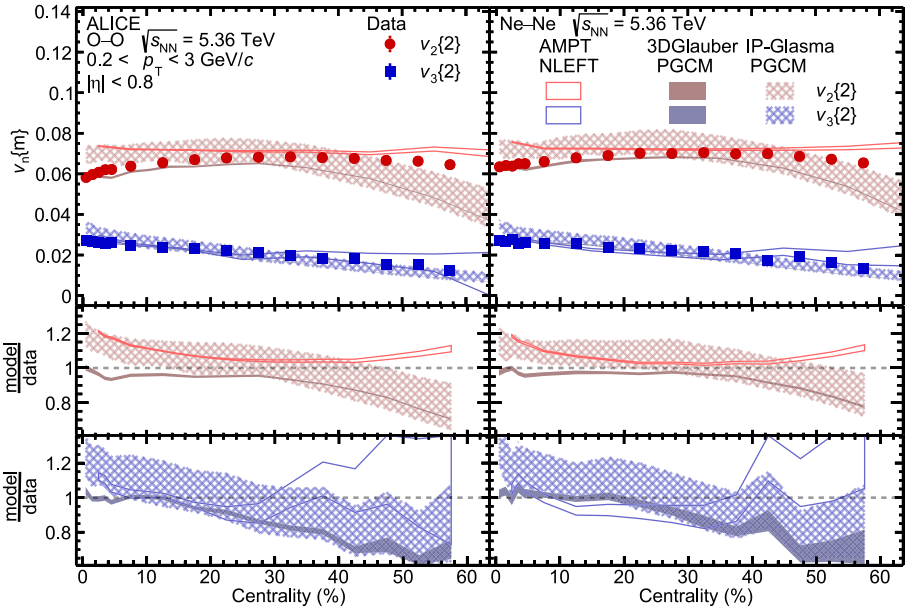


FIG. 6. Charged particle $v_2\{2\}$ and $v_3\{2\}$ as a function of centrality in OO (left) and Ne–Ne (right) collisions. The data points are the same as those in Fig. 2. The measurements are compared with IP-Glasma + JIMWLK + MUSIC + UrQMD [93] and 3DGlauber + MUSIC + UrQMD [94] calculations with PGCM input, as well as AMPT [58] with NLEFT input.

effects of the system evolution and highlights the initial fluctuations. Previous studies have shown that the ratio is sensitive to the α-cluster configuration and compactness of ^{16}O in relativistic OO collisions [57,58,102,103]. In Fig. 5, the centrality dependence of $v_2\{4\}/v_2\{2\}$ in OO and Ne–Ne collisions, as well as the ratio between the two collision systems, are presented. The $v_2\{4\}/v_2\{2\}$ is lowest in central collisions and increases with larger centrality. A similar trend is observed in both Xe–Xe [10] and Pb–Pb collisions [9], albeit with larger magnitudes as the larger flow fluctuations in the small light-ion collisions reduce the $v_2\{4\}/v_2\{2\}$ ratio. The double ratio of $v_2\{4\}/v_2\{2\}$ between Ne–Ne and OO is slightly below unity in non-central collisions due to the larger flow fluctuations in the smaller OO collisions. In central collisions, the double ratio increases due to the effect of nuclear structure. The ^{20}Ne nuclei have larger deformation, and thus Ne–Ne collisions produce stronger v_2 than OO collisions, while the flow fluctuations remain similar. Note that the $v_2\{4\}/v_2\{2\}$ ratio in OO and Ne–Ne would decrease by a few percentages if centrality is redefined from an estimation based on the multiplicity at forward rapidity (default option) to one based on midrapidity, consistent with what is discussed in Fig. 2.

In Fig. 6, the measurements of flow coefficients, identical to those shown in Fig. 2, are compared with hydrodynamic calculations from the 3D-Glauber + MUSIC + UrQMD and IP-Glasma + JIMWLK + MUSIC + UrQMD frameworks, as well as with calculations from the AMPT transport model. The hydrodynamic calculations are both based on PGCM nuclear structure inputs, whereas the AMPT model uses nuclear structure from NLEFT. The IP-Glasma-based calculations overestimate the v_2 measurements in the most central collisions, 0%–10%; underestimate them at centralities above 50%; and show reasonable agreement with the data across intermediate centralities. In contrast, the 3D-Glauber-based calculations consistently underestimate the v_2 measurements, whereas the AMPT model shows no clear centrality dependence and systematically overestimates the v_2 values across the entire centrality range. All presented model calculations exhibit reasonable agreement with the measured v_3, although the uncertainties remain large.

I. J. Abualrob,[114] S. Acharya,[50] G. Aglieri Rinella,[32] L. Aglietta,[24] N. Agrawal,[25] Z. Ahammed,[134] S. Ahmad,[15] I. Ahuja,[36] Z. Akbar,[81] A. Akindinov,[140] V. Akishina,[38] M. Al-Turany,[96] D. Aleksandrov,[140] B. Alessandro,[56] R. Alfaro Molina,[67] B. Ali,[15] A. Alici,[25,†] A. Alkin,[102] J. Alme,[20] G. Alocco,[24] T. Alt,[64] I. Altsybeev,[94] C. Andrei,[45] N. Andreou,[113] A. Andronic,[125] E. Andronov,[140] M. Angeletti,[32] V. Anguelov,[93] F. Antinori,[54]

P. Antonioli,[51] N. Apadula,[72] H. Appelshäuser,[64] S. Arcelli,[25,†] R. Arnaldi,[56] I. C. Arsene,[19] M. Arslandok,[137] A. Augustinus,[32] R. Averbeck,[96] M. D. Azmi,[15] H. Baba,[123] A. R. J. Babu,[136] A. Badalà,[53] J. Bae,[102] Y. Bae,[102] Y. W. Baek,[40] X. Bai,[118] R. Bailhache,[64] Y. Bailung,[48] R. Bala,[90] A. Baldisseri,[129] B. Balis,[2] S. Bangalia,[116] Z. Banoo,[90] V. Barbasova,[36] F. Barile,[31] L. Barioglio,[56] M. Barlou,[24,77] B. Barman,[41] G. G. Barnaföldi,[46] L. S. Barnby,[113] E. Barreau,[101] V. Barret,[126] L. Barreto,[108] K. Barth,[32] E. Bartsch,[64] N. Bastid,[126] G. Batigne,[101] D. Battistini,[94] B. Batyunya,[141] D. Bauri,[47] J. L. Bazo Alba,[100] I. G. Bearden,[82] P. Becht,[96] D. Behera,[48] S. Behera,[47] I. Belikov,[128] V. D. Bella,[128] F. Bellini,[25] R. Bellwied,[114] L. G. E. Beltran,[107] Y. A. V. Beltran,[44] G. Bencedi,[46] A. Bensaoula,[114] S. Beole,[24] Y. Berdnikov,[140] A. Berdnikova,[93] L. Bergmann,[72,93] L. Bernardinis,[23] L. Betev,[32] P. P. Bhaduri,[134] T. Bhalla,[89] A. Bhasin,[90] B. Bhattacharjee,[41] S. Bhattarai,[116] L. Bianchi,[24] J. Bielčík,[34] J. Bielčíková,[85] A. Bilandzic,[94] A. Binoy,[116] G. Biro,[46] S. Biswas,[4] D. Blau,[140] M. B. Blidaru,[96] N. Bluhme,[38] C. Blume,[64] F. Bock,[86] T. Bodova,[20] L. Boldizsár,[46] M. Bombara,[36] P. M. Bond,[32] G. Bonomi,[55,133] H. Borel,[129] A. Borissov,[140] A. G. Borquez Carcamo,[93] E. Botta,[24] Y. E. M. Bouziani,[64] D. C. Brandibur,[63] L. Bratrud,[64] P. Braun-Munzinger,[96] M. Bregant,[108] M. Broz,[34] G. E. Bruno,[31,95] V. D. Buchakchiev,[35] M. D. Buckland,[84] H. Buesching,[64] S. Bufalino,[29] P. Buhler,[74] N. Burmasov,[141] Z. Buthelezi,[68,122] A. Bylinkin,[20] J. C. Cabanillas Noris,[107] M. F. T. Cabrera,[114] H. Caines,[137] A. Caliva,[28] E. Calvo Villar,[100] J. M. M. Camacho,[107] P. Camerini,[23] M. T. Camerlingo,[50] F. D. M. Canedo,[108] S. Cannito,[23] S. L. Cantway,[137] M. Carabas,[111] F. Carnesecchi,[32] C. Carr,[99] L. A. D. Carvalho,[108] J. Castillo Castellanos,[129] M. Castoldi,[32] F. Catalano,[32] S. Cattaruzzi,[23] R. Cerri,[24] I. Chakaberia,[72] P. Chakraborty,[135] J. W. O. Chan,[114] S. Chandra,[134] S. Chapeland,[32] M. Chartier,[117] S. Chattopadhay,[134] M. Chen,[39] T. Cheng,[6] C. Cheshkov,[127] D. Chiappara,[27] V. Chibante Barroso,[32] D. D. Chinellato,[74] F. Chinu,[24] E. S. Chizzali,[94,‡] J. Cho,[58] S. Cho,[58] P. Chochula,[32] Z. A. Chochulska,[135,§] P. Christakoglou,[83] C. H. Christensen,[82] P. Christiansen,[73] T. Chujo,[124] M. Ciacco,[24] C. Cicalo,[52] G. Cimador,[24] F. Cindolo,[51] F. Colamaria,[50] D. Colella,[31] A. Colelli,[31] M. Colocci,[25] M. Concas,[32] G. Conesa Balbastre,[71] Z. Conesa del Valle,[130] G. Contin,[23] J. G. Contreras,[34] M. L. Coquet,[101] P. Cortese,[56,132] M. R. Cosentino,[110] F. Costa,[32] S. Costanza,[21] P. Crochet,[126] M. M. Czarnynoga,[135] A. Dainese,[54] G. Dange,[38] M. C. Danisch,[16] A. Danu,[63] P. Das,[32] S. Das,[4] A. R. Dash,[125] S. Dash,[47] A. De Caro,[28] G. de Cataldo,[50] J. de Cuveland,[38] A. De Falco,[22] D. De Gruttola,[28] N. De Marco,[56] C. De Martin,[23] S. De Pasquale,[28] R. Deb,[133] R. Del Grande,[94] L. Dello Stritto,[32] G. G. A. de Souza,[108,‖] P. Dhankher,[18] D. Di Bari,[31] M. Di Costanzo,[29] A. Di Mauro,[32] B. Di Ruzza,[50,131,†] B. Diab,[32] Y. Ding,[6] J. Ditzel,[64] R. Divià,[32] U. Dmitrieva,[56] A. Dobrin,[63] B. Dönigus,[64] L. Döpper,[42] J. M. Dubinski,[135] A. Dubla,[96] P. Dupieux,[126] N. Dzalaiova,[13] T. M. Eder,[125] R. J. Ehlers,[72] F. Eisenhut,[64] R. Ejima,[91] D. Elia,[50] B. Erazmus,[101] F. Ercolessi,[25] B. Espagnon,[130] G. Eulisse,[32] D. Evans,[99] L. Fabbietti,[94] M. Faggin,[32] J. Faivre,[71] F. Fan,[6] W. Fan,[114] T. Fang,[6] A. Fantoni,[49] M. Fasel,[86] A. Feliciello,[56] W. Feng,[6] G. Feofilov,[140] A. Fernández Téllez,[44] L. Ferrandi,[108] A. Ferrero,[129] C. Ferrero,[56,¶] A. Ferretti,[24] V. J. G. Feuillard,[93] D. Finogeev,[141] F. M. Fionda,[52] A. N. Flores,[106] S. Foertsch,[68] I. Fokin,[93] S. Fokin,[140] U. Follo,[56,¶] R. Forynski,[113] E. Fragiacomo,[57] H. Fribert,[94] U. Fuchs,[32] N. Funicello,[28] C. Furget,[71] A. Furs,[141] T. Fusayasu,[97] J. J. Gaardhøje,[82] M. Gagliardi,[24] A. M. Gago,[100] T. Gahlaut,[47] C. D. Galvan,[107] S. Gami,[79] P. Ganoti,[77] C. Garabatos,[96] J. M. Garcia,[44] T. García Chávez,[44] E. Garcia-Solis,[9] S. Garetti,[130] C. Gargiulo,[32] P. Gasik,[96] H. M. Gaur,[38] A. Gautam,[116] M. B. Gay Ducati,[66] M. Germain,[101] R. A. Gernhaeuser,[94] C. Ghosh,[134] M. Giacalone,[32] G. Gioachin,[29] S. K. Giri,[134] P. Giubellino,[56] P. Giubilato,[27] P. Glässel,[93] E. Glimos,[121] V. Gonzalez,[136] M. Gorgon,[2] K. Goswami,[48] S. Gotovac,[33] V. Grabski,[67] L. K. Graczykowski,[135] E. Grecka,[85] A. Grelli,[59] C. Grigoras,[32] V. Grigoriev,[140] S. Grigoryan,[1,141] O. S. Groettvik,[32] F. Grosa,[32] S. Gross-Bölting,[96] J. F. Grosse-Oetringhaus,[32] R. Grosso,[96] D. Grund,[34] N. A. Grunwald,[93] R. Guernane,[71] M. Guilbaud,[101] K. Gulbrandsen,[82] J. K. Gumprecht,[74] T. Gündem,[64] T. Gunji,[123] J. Guo,[10] W. Guo,[6] A. Gupta,[90] R. Gupta,[90] R. Gupta,[48] K. Gwizdziel,[135] L. Gyulai,[46] C. Hadjidakis,[130] F. U. Haider,[90] S. Haidlova,[34] M. Haldar,[4] H. Hamagaki,[75] Y. Han,[139] B. G. Hanley,[136] R. Hannigan,[106] J. Hansen,[73] J. W. Harris,[137] A. Harton,[9] M. V. Hartung,[64] A. Hasan,[120] H. Hassan,[115] D. Hatzifotiadou,[51] P. Hauer,[42] L. B. Havener,[137] E. Hellbär,[32] H. Helstrup,[37] M. Hemmer,[64] S. G. Hernandez,[114] G. Herrera Corral,[8] K. F. Hetland,[37] B. Heybeck,[64] H. Hillemanns,[32] B. Hippolyte,[128] I. P. M. Hobus,[83] F. W. Hoffmann,[38] B. Hofman,[59] Y. Hong,[58] A. Horzyk,[2] Y. Hou,[6,11,96] P. Hristov,[32] P. Huhn,[64] L. M. Huhta,[115]

T. J. Humanic,[87] V. Humlova,[34] A. Hutson,[114] D. Hutter,[38] M. C. Hwang,[18] R. Ilkaev,[140] M. Inaba,[124] M. Ippolitov,[140] A. Isakov,[83] T. Isidori,[116] M. S. Islam,[47] M. Ivanov,[96] M. Ivanov,[13] K. E. Iversen,[73] M. Jablonski,[2] B. Jacak,[18,72] N. Jacazio,[25] P. M. Jacobs,[72] S. Jadlovska,[104] J. Jadlovsky,[104] S. Jaelani,[81] C. Jahnke,[109] M. J. Jakubowska,[135] E. P. Jamro,[2] D. M. Janik,[34] M. A. Janik,[135] C. A. Jauch,[96] S. Ji,[16] Y. Ji,[96] S. Jia,[82] T. Jiang,[10] A. A. P. Jimenez,[65] S. Jin,[10] F. Jonas,[72] D. M. Jones,[117] J. M. Jowett,[32,96] J. Jung,[64] M. Jung,[64] A. Junique,[32] A. Jusko,[99] J. Kaewjai,[103] P. Kalinak,[60] A. Kalweit,[32] H. Kang,[12] A. Karasu Uysal,[138] N. Karatzenis,[99] O. Karavichev,[140] T. Karavicheva,[140] M. J. Karwowska,[135] V. Kashyap,[79] M. Keil,[32] B. Ketzer,[42] J. Keul,[64] S. S. Khade,[48] A. M. Khan,[118] A. Khanzadeev,[140] Y. Kharlov,[140] A. Khatun,[116] A. Khuntia,[51] Z. Khuranova,[64] B. Kileng,[37] B. Kim,[102] D. J. Kim,[115] D. Kim,[102] E. J. Kim,[69] G. Kim,[58] H. Kim,[58] J. Kim,[139] J. Kim,[58] J. Kim,[139] J. Kim,[32] M. Kim,[18] S. Kim,[17] T. Kim,[139] K. Kimura,[91] J. T. Kinner,[125] S. Kirsch,[64] I. Kisel,[38] S. Kiselev,[140] A. Kisiel,[135] J. L. Klay,[5] J. Klein,[32] S. Klein,[72] C. Klein-Bösing,[125] M. Kleiner,[64] A. Kluge,[32] M. B. Knuesel,[137] C. Kobdaj,[103] R. Kohara,[123] A. Kondratyev,[141] N. Kondratyeva,[140] J. Konig,[64] P. J. Konopka,[32] G. Kornakov,[135] M. Korwieser,[94] S. D. Koryciak,[2] C. Koster,[83] A. Kotliarov,[85] N. Kovacic,[88] V. Kovalenko,[140] M. Kowalski,[105] V. Kozhuharov,[35] G. Kozlov,[38] I. Králik,[60] A. Kravčáková,[36] L. Krcal,[32] M. Krivda,[60,99] F. Krizek,[85] K. Krizkova Gajdosova,[34] C. Krug,[66] M. Krüger,[64] E. Kryshen,[140] V. Kučera,[58] C. Kuhn,[128] T. Kumaoka,[124] D. Kumar,[134] L. Kumar,[89] N. Kumar,[89] S. Kumar,[50] S. Kundu,[32] M. Kuo,[124] P. Kurashvili,[78] A. B. Kurepin,[140] S. Kurita,[91] A. Kuryakin,[140] S. Kushpil,[85] A. Kuznetsov,[141] M. J. Kweon,[58] Y. Kwon,[139] S. L. La Pointe,[38] P. La Rocca,[26] A. Lakrathok,[103] S. Lambert,[101] A. R. Landou,[71] R. Langoy,[120] E. Laudi,[32] L. Lautner,[94] R. A. N. Laveaga,[107] R. Lavicka,[74] R. Lea,[55,133] J. B. Lebert,[38] H. Lee,[102] S. Lee,[58] I. Legrand,[45] G. Legras,[125] A. M. Lejeune,[34] T. M. Lelek,[2] I. León Monzón,[107] M. M. Lesch,[94] P. Lévai,[46] M. Li,[6] P. Li,[10] X. Li,[10] B. E. Liang-Gilman,[18] J. Lien,[120] R. Lietava,[99] I. Likmeta,[114] B. Lim,[56] H. Lim,[16] S. H. Lim,[16] S. Lin,[10] V. Lindenstruth,[38] C. Lippmann,[96] D. Liskova,[104] D. H. Liu,[6] J. Liu,[117] Y. Liu,[6] G. S. S. Liveraro,[109] I. M. Lofnes,[20] C. Loizides,[86] S. Lokos,[105] J. Lömker,[59] X. Lopez,[126] E. López Torres,[7] C. Lotteau,[127] P. Lu,[118] W. Lu,[6] Z. Lu,[10] O. Lubynets,[96] F. V. Lugo,[67] J. Luo,[39] G. Luparello,[57] J. M. Friedrich,[94] Y. G. Ma,[39] M. Mager,[32] M. Mahlein,[94] A. Maire,[128] E. Majerz,[2] M. V. Makariev,[35] G. Malfattore,[51] N. M. Malik,[90] N. Malik,[15] S. K. Malik,[90] D. Mallick,[130] N. Mallick,[115] G. Mandaglio,[30,53] S. K. Mandal,[78] A. Manea,[63] R. Manhart,[94] V. Manko,[140] A. K. Manna,[48] F. Manso,[126] G. Mantzaridis,[94] V. Manzari,[50] Y. Mao,[6] R. W. Marcjan,[2] G. V. Margagliotti,[23] A. Margotti,[51] A. Marín,[96] C. Markert,[106] P. Martinengo,[32] M. I. Martínez,[44] M. P. P. Martins,[32,108] S. Masciocchi,[96] M. Masera,[24] A. Masoni,[52] L. Massacrier,[130] O. Massen,[59] A. Mastroserio,[50,131] L. Mattei,[24,126] S. Mattiazzo,[27] A. Matyja,[105] J. L. Mayo,[106] F. Mazzaschi,[32] M. Mazzilli,[31,114] Y. Melikyan,[43] M. Melo,[108] A. Menchaca-Rocha,[67] J. E. M. Mendez,[65] E. Meninno,[74] M. W. Menzel,[32,93] M. Meres,[13] L. Micheletti,[56] D. Mihai,[111] D. L. Mihaylov,[94] A. U. Mikalsen,[20] K. Mikhaylov,[140,141] L. Millot,[71] N. Minafra,[116,**] D. Miśkowiec,[96] A. Modak,[57,133] B. Mohanty,[79] M. Mohisin Khan,[15,††] M. A. Molander,[43] M. M. Mondal,[79] S. Monira,[135] D. A. Moreira De Godoy,[125] A. Morsch,[32] T. Mrnjavac,[32] S. Mrozinski,[64] V. Muccifora,[49] S. Muhuri,[134] A. Mulliri,[22] M. G. Munhoz,[108] R. H. Munzer,[64] H. Murakami,[123] L. Musa,[32] J. Musinsky,[60] J. W. Myrcha,[135] B. Naik,[122] A. I. Nambrath,[18] B. K. Nandi,[47] R. Nania,[51] E. Nappi,[50] A. F. Nassirpour,[17] V. Nastase,[111] A. Nath,[93] N. F. Nathanson,[82] K. Naumov,[18] A. Neagu,[19] L. Nellen,[65] R. Nepeivoda,[73] S. Nese,[19] N. Nicassio,[31] B. S. Nielsen,[82] E. G. Nielsen,[82] S. Nikolaev,[140] V. Nikulin,[140] F. Noferini,[51] S. Noh,[12] P. Nomokonov,[141] J. Norman,[117] N. Novitzky,[86] A. Nyanin,[140] J. Nystrand,[20] M. R. Ockleton,[117] M. Ogino,[75] J. Oh,[16] S. Oh,[17] A. Ohlson,[73] M. Oida,[91] V. A. Okorokov,[140] C. Oppedisano,[56] A. Ortiz Velasquez,[65] H. Osanai,[75] J. Otwinowski,[105] M. Oya,[91] K. Oyama,[75] S. Padhan,[47,133] D. Pagano,[55,133] G. Paić,[65] S. Paisano-Guzmán,[44] A. Palasciano,[50,95] I. Panasenko,[73] P. Panigrahi,[47] C. Pantouvakis,[27] H. Park,[124] J. Park,[124] S. Park,[102] T. Y. Park,[139] J. E. Parkkila,[135] P. B. Pati,[82] Y. Patley,[47] R. N. Patra,[50] P. Paudel,[116] B. Paul,[134] H. Pei,[6] T. Peitzmann,[59] X. Peng,[11,54] M. Pennisi,[24] S. Perciballi,[24] D. Peresunko,[140] G. M. Perez,[7] Y. Pestov,[140] M. Petrovici,[45] S. Piano,[57] M. Pikna,[13] P. Pillot,[101] O. Pinazza,[32,51] C. Pinto,[32] S. Pisano,[49] M. Płoskoń,[72] M. Planinic,[88] D. K. Plociennik,[2] M. G. Poghosyan,[86] B. Polichtchouk,[140] S. Politano,[32] N. Poljak,[88] A. Pop,[45] S. Porteboeuf-Houssais,[126] J. S. Potgieter,[112] I. Y. Pozos,[44] K. K. Pradhan,[48] S. K. Prasad,[4] S. Prasad,[48] R. Preghenella,[51] F. Prino,[56] C. A. Pruneau,[136] I. Pshenichnov,[140] M. Puccio,[32] S. Pucillo,[24,28] S. Pulawski,[119]

L. Quaglia,[24] A. M. K. Radhakrishnan,[48] S. Ragoni,[14] A. Rai,[137] A. Rakotozafindrabe,[129] N. Ramasubramanian,[127] L. Ramello,[56,132] C. O. Ramírez-Álvarez,[44] M. Rasa,[26] S. S. Räsänen,[43] R. Rath,[96] M. P. Rauch,[20] I. Ravasenga,[32] K. F. Read,[86,121] C. Reckziegel,[110] A. R. Redelbach,[38] K. Redlich,[78,‡‡] H. D. Regules-Medel,[44] A. Rehman,[20] F. Reidt,[32] H. A. Reme-Ness,[37] K. Reygers,[93] R. Ricci,[28] M. Richter,[20] A. A. Riedel,[94] W. Riegler,[32] A. G. Riffero,[24] M. Rignanese,[27] C. Ripoli,[28] C. Ristea,[63] M. V. Rodriguez,[32] M. Rodríguez Cahuantzi,[44] K. Røed,[19] R. Rogalev,[140] E. Rogochaya,[141] D. Rohr,[32] D. Röhrich,[20] S. Rojas Torres,[34] P. S. Rokita,[135] G. Romanenko,[25] F. Ronchetti,[32] D. Rosales Herrera,[44] K. Roslon,[135] A. Rossi,[54] A. Roy,[48] S. Roy,[47] N. Rubini,[51] J. A. Rudolph,[83] D. Ruggiano,[135] R. Rui,[23] P. G. Russek,[2] A. Rustamov,[80] Y. Ryabov,[140] A. Rybicki,[105] L. C. V. Ryder,[116] G. Ryu,[70] J. Ryu,[16] W. Rzesa,[94,135] B. Sabiu,[51] R. Sadek,[72] S. Sadhu,[42] S. Sadovsky,[140] A. Saha,[31] S. Saha,[79] B. Sahoo,[48] R. Sahoo,[48] D. Sahu,[65] P. K. Sahu,[61] J. Saini,[134] S. Sakai,[124] S. Sambyal,[90] D. Samitz,[74] I. Sanna,[32] T. B. Saramela,[108] D. Sarkar,[82] V. Sarritzu,[22] V. M. Sarti,[94] U. Savino,[24] S. Sawan,[79] E. Scapparone,[51] J. Schambach,[86] H. S. Scheid,[32] C. Schiaua,[45] R. Schicker,[93] F. Schlepper,[32,93] A. Schmah,[96] C. Schmidt,[96] M. Schmidt,[92] N. V. Schmidt,[86] A. R. Schmier,[121] J. Schoengarth,[64] R. Schotter,[74] A. Schröter,[38] J. Schukraft,[32] K. Schweda,[96] G. Scioli,[25] E. Scomparin,[56] J. E. Seger,[14] Y. Sekiguchi,[123] D. Sekihata,[123] M. Selina,[83] I. Selyuzhenkov,[96] S. Senyukov,[128] J. J. Seo,[93] D. Serebryakov,[140] L. Serkin,[65,§§] L. Šerkšnytė,[94] A. Sevcenco,[63] T. J. Shaba,[68] A. Shabetai,[101] R. Shahoyan,[32] B. Sharma,[90] D. Sharma,[47] H. Sharma,[54] M. Sharma,[90] S. Sharma,[90] T. Sharma,[41] U. Sharma,[90] O. Sheibani,[136] K. Shigaki,[91] M. Shimomura,[76] S. Shirinkin,[140] Q. Shou,[39] Y. Sibiriak,[140] S. Siddhanta,[52] T. Siemiarczuk,[78] T. F. Silva,[108] W. D. Silva,[108] D. Silvermyr,[73] T. Simantathammakul,[103] R. Simeonov,[35] B. Singh,[90] B. Singh,[94] K. Singh,[48] R. Singh,[79] R. Singh,[54,96] S. Singh,[15] V. K. Singh,[134] V. Singhal,[134] T. Sinha,[98] B. Sitar,[13] M. Sitta,[56,132] T. B. Skaali,[19] G. Skorodumovs,[93] N. Smirnov,[137] K. L. Smith,[16] R. J. M. Snellings,[59] E. H. Solheim,[19] C. Sonnabend,[32,96] J. M. Sonneveld,[83] F. Soramel,[27] A. B. Soto-Hernandez,[87] R. Spijkers,[83] C. Sporleder,[115] I. Sputowska,[105] J. Staa,[73] J. Stachel,[93] L. L. Stahl,[108] I. Stan,[63] T. Stellhorn,[125] S. F. Stiefelmaier,[93] D. Stocco,[101] I. Storehaug,[19] N. J. Strangmann,[64] P. Stratmann,[125] S. Strazzi,[25] A. Sturniolo,[30,53] Y. Su,[6] A. A. P. Suaide,[108] C. Suire,[130] A. Suiu,[111] M. Sukhanov,[141] M. Suljic,[32] R. Sultanov,[140] V. Sumberia,[90] S. Sumowidagdo,[81] N. B. Sundstrom,[59] L. H. Tabares,[7] S. F. Taghavi,[94] J. Takahashi,[109] M. A. Talamantes Johnson,[44] G. J. Tambave,[79] Z. Tang,[118] J. Tanwar,[89] J. D. Tapia Takaki,[116] N. Tapus,[111] L. A. Tarasovicova,[36] M. G. Tarzila,[45] A. Tauro,[32] A. Tavira García,[130] G. Tejeda Muñoz,[44] L. Terlizzi,[24] C. Terrevoli,[50] D. Thakur,[24] S. Thakur,[4] M. Thogersen,[19] D. Thomas,[106] N. Tiltmann,[32,125] A. R. Timmins,[114] A. Toia,[64] R. Tokumoto,[91] S. Tomassini,[25] K. Tomohiro,[91] Q. Tong,[6] N. Topilskaya,[140] V. V. Torres,[101] A. Trifiró,[30,53] T. Triloki,[95] A. S. Triolo,[32,53] S. Tripathy,[32] T. Tripathy,[126] S. Trogolo,[24] V. Trubnikov,[3] W. H. Trzaska,[115] T. P. Trzcinski,[135] C. Tsolanta,[19] R. Tu,[39] A. Tumkin,[140] R. Turrisi,[54] T. S. Tveter,[19] K. Ullaland,[20] B. Ulukutlu,[94] S. Upadhyaya,[105] A. Uras,[127] M. Urioni,[23] G. L. Usai,[22] M. Vaid,[90] M. Vala,[36] N. Valle,[55] L. V. R. van Doremalen,[59] M. van Leeuwen,[83] C. A. van Veen,[93] R. J. G. van Weelden,[83] D. Varga,[46] Z. Varga,[137] P. Vargas Torres,[65] M. Vasileiou,[77] O. Vázquez Doce,[49] O. Vazquez Rueda,[114] V. Vechernin,[140] P. Veen,[129] E. Vercellin,[24] R. Verma,[47] R. Vértesi,[46] M. Verweij,[59] L. Vickovic,[33] Z. Vilakazi,[122] O. Villalobos Baillie,[99] A. Villani,[23] A. Vinogradov,[140] T. Virgili,[28] M. M. O. Virta,[115] A. Vodopyanov,[141] M. A. Völkl,[99] S. A. Voloshin,[136] G. Volpe,[31] B. von Haller,[32] I. Vorobyev,[32] N. Vozniuk,[141] J. Vrláková,[36] J. Wan,[39] C. Wang,[39] D. Wang,[39] Y. Wang,[118] Y. Wang,[39] Y. Wang,[6] Z. Wang,[39] F. Weiglhofer,[32,38] S. C. Wenzel,[32] J. P. Wessels,[125] P. K. Wiacek,[2] J. Wiechula,[64] J. Wikne,[19] G. Wilk,[78] J. Wilkinson,[96] G. A. Willems,[125] B. Windelband,[93] J. Witte,[93] M. Wojnar,[2] J. R. Wright,[106] C.-T. Wu,[6,27] W. Wu,[39,94] Y. Wu,[118] K. Xiong,[39] Z. Xiong,[118] L. Xu,[6,127] R. Xu,[6] A. Yadav,[42] A. K. Yadav,[134] Y. Yamaguchi,[91] S. Yang,[58] S. Yang,[20] S. Yano,[91] Z. Ye,[72] E. R. Yeats,[18] J. Yi,[6] R. Yin,[39] Z. Yin,[6] I.-K. Yoo,[16] J. H. Yoon,[58] H. Yu,[12] S. Yuan,[20] A. Yuncu,[93] V. Zaccolo,[23] C. Zampolli,[32] F. Zanone,[93] N. Zardoshti,[32] P. Závada,[62] B. Zhang,[93] C. Zhang,[129] L. Zhang,[39] M. Zhang,[6,126] M. Zhang,[6,27] S. Zhang,[39] X. Zhang,[6] Y. Zhang,[118] Y. Zhang,[118] Z. Zhang,[6] V. Zherebchevskii,[140] Y. Zhi,[10] D. Zhou,[6] Y. Zhou,[82] J. Zhu,[39] S. Zhu,[96,118] Y. Zhu,[6] A. Zingaretti,[27] S. C. Zugravel,[56] and N. Zurlo[55,133]

(ALICE Collaboration)

[1]A.I. Alikhanyan National Science Laboratory (Yerevan Physics Institute) Foundation, Yerevan, Armenia
[2]AGH University of Krakow, Cracow, Poland
[3]Bogolyubov Institute for Theoretical Physics, National Academy of Sciences of Ukraine, Kyiv, Ukraine
[4]Bose Institute, Department of Physics and Centre for Astroparticle Physics and Space Science (CAPSS), Kolkata, India
[5]California Polytechnic State University, San Luis Obispo, California, USA
[6]Central China Normal University, Wuhan, China
[7]Centro de Aplicaciones Tecnológicas y Desarrollo Nuclear (CEADEN), Havana, Cuba
[8]Centro de Investigación y de Estudios Avanzados (CINVESTAV), Mexico City and Mérida, Mexico
[9]Chicago State University, Chicago, Illinois, USA
[10]China Nuclear Data Center, China Institute of Atomic Energy, Beijing, China
[11]China University of Geosciences, Wuhan, China
[12]Chungbuk National University, Cheongju, Republic of Korea
[13]Comenius University Bratislava, Faculty of Mathematics, Physics and Informatics, Bratislava, Slovak Republic
[14]Creighton University, Omaha, Nebraska, USA
[15]Department of Physics, Aligarh Muslim University, Aligarh, India
[16]Department of Physics, Pusan National University, Pusan, Republic of Korea
[17]Department of Physics, Sejong University, Seoul, Republic of Korea
[18]Department of Physics, University of California, Berkeley, California, USA
[19]Department of Physics, University of Oslo, Oslo, Norway
[20]Department of Physics and Technology, University of Bergen, Bergen, Norway
[21]Dipartimento di Fisica, Università di Pavia, Pavia, Italy
[22]Dipartimento di Fisica dell'Università and Sezione INFN, Cagliari, Italy
[23]Dipartimento di Fisica dell'Università and Sezione INFN, Trieste, Italy
[24]Dipartimento di Fisica dell'Università and Sezione INFN, Turin, Italy
[25]Dipartimento di Fisica e Astronomia dell'Università and Sezione INFN, Bologna, Italy
[26]Dipartimento di Fisica e Astronomia dell'Università and Sezione INFN, Catania, Italy
[27]Dipartimento di Fisica e Astronomia dell'Università and Sezione INFN, Padova, Italy
[28]Dipartimento di Fisica "E.R. Caianiello" dell'Università and Gruppo Collegato INFN, Salerno, Italy
[29]Dipartimento DISAT del Politecnico and Sezione INFN, Turin, Italy
[30]Dipartimento di Scienze MIFT, Università di Messina, Messina, Italy
[31]Dipartimento Interateneo di Fisica 'M. Merlin' and Sezione INFN, Bari, Italy
[32]European Organization for Nuclear Research (CERN), Geneva, Switzerland
[33]Faculty of Electrical Engineering, Mechanical Engineering and Naval Architecture, University of Split, Split, Croatia
[34]Faculty of Nuclear Sciences and Physical Engineering, Czech Technical University in Prague, Prague, Czechia
[35]Faculty of Physics, Sofia University, Sofia, Bulgaria
[36]Faculty of Science, P.J. Šafárik University, Košice, Slovak Republic
[37]Faculty of Technology, Environmental and Social Sciences, Bergen, Norway
[38]Frankfurt Institute for Advanced Studies, Johann Wolfgang Goethe-Universität Frankfurt, Frankfurt, Germany
[39]Fudan University, Shanghai, China
[40]Gangneung-Wonju National University, Gangneung, Republic of Korea
[41]Gauhati University, Department of Physics, Guwahati, India
[42]Helmholtz-Institut für Strahlen- und Kernphysik, Rheinische Friedrich-Wilhelms-Universität Bonn, Bonn, Germany
[43]Helsinki Institute of Physics (HIP), Helsinki, Finland
[44]High Energy Physics Group, Universidad Autónoma de Puebla, Puebla, Mexico
[45]Horia Hulubei National Institute of Physics and Nuclear Engineering, Bucharest, Romania
[46]HUN-REN Wigner Research Centre for Physics, Budapest, Hungary
[47]Indian Institute of Technology Bombay (IIT), Mumbai, India
[48]Indian Institute of Technology Indore, Indore, India
[49]INFN, Laboratori Nazionali di Frascati, Frascati, Italy
[50]INFN, Sezione di Bari, Bari, Italy
[51]INFN, Sezione di Bologna, Bologna, Italy
[52]INFN, Sezione di Cagliari, Cagliari, Italy
[53]INFN, Sezione di Catania, Catania, Italy
[54]INFN, Sezione di Padova, Padova, Italy
[55]INFN, Sezione di Pavia, Pavia, Italy
[56]INFN, Sezione di Torino, Turin, Italy
[57]INFN, Sezione di Trieste, Trieste, Italy
[58]Inha University, Incheon, Republic of Korea
[59]Institute for Gravitational and Subatomic Physics (GRASP), Utrecht University/Nikhef, Utrecht, Netherlands

[60]Institute of Experimental Physics, Slovak Academy of Sciences, Košice, Slovak Republic
[61]Institute of Physics, Homi Bhabha National Institute, Bhubaneswar, India
[62]Institute of Physics of the Czech Academy of Sciences, Prague, Czech Republic
[63]Institute of Space Science (ISS), Bucharest, Romania
[64]Institut für Kernphysik, Johann Wolfgang Goethe-Universität Frankfurt, Frankfurt, Germany
[65]Instituto de Ciencias Nucleares, Universidad Nacional Autónoma de México, Mexico City, Mexico
[66]Instituto de Física, Universidade Federal do Rio Grande do Sul (UFRGS), Porto Alegre, Brazil
[67]Instituto de Física, Universidad Nacional Autónoma de México, Mexico City, Mexico
[68]iThemba LABS, National Research Foundation, Somerset West, South Africa
[69]Jeonbuk National University, Jeonju, Republic of Korea
[70]Korea Institute of Science and Technology Information, Daejeon, Republic of Korea
[71]Laboratoire de Physique Subatomique et de Cosmologie, Université Grenoble-Alpes, CNRS-IN2P3, Grenoble, France
[72]Lawrence Berkeley National Laboratory, Berkeley, California, USA
[73]Lund University Department of Physics, Division of Particle Physics, Lund, Sweden
[74]Marietta Blau Institute, Vienna, Austria
[75]Nagasaki Institute of Applied Science, Nagasaki, Japan
[76]Nara Women's University (NWU), Nara, Japan
[77]National and Kapodistrian University of Athens, School of Science, Department of Physics, Athens, Greece
[78]National Centre for Nuclear Research, Warsaw, Poland
[79]National Institute of Science Education and Research, Homi Bhabha National Institute, Jatni, India
[80]National Nuclear Research Center, Baku, Azerbaijan
[81]National Research and Innovation Agency - BRIN, Jakarta, Indonesia
[82]Niels Bohr Institute, University of Copenhagen, Copenhagen, Denmark
[83]Nikhef, National institute for subatomic physics, Amsterdam, Netherlands
[84]Nuclear Physics Group, STFC Daresbury Laboratory, Daresbury, United Kingdom
[85]Nuclear Physics Institute of the Czech Academy of Sciences, Husinec-Řež, Czech Republic
[86]Oak Ridge National Laboratory, Oak Ridge, Tennessee, USA
[87]Ohio State University, Columbus, Ohio, USA
[88]Physics department, Faculty of science, University of Zagreb, Zagreb, Croatia
[89]Physics Department, Panjab University, Chandigarh, India
[90]Physics Department, University of Jammu, Jammu, India
[91]Physics Program and International Institute for Sustainability with Knotted Chiral Meta Matter (WPI-SKCM^2), Hiroshima University, Hiroshima, Japan
[92]Physikalisches Institut, Eberhard-Karls-Universität Tübingen, Tubingen, Germany
[93]Physikalisches Institut, Ruprecht-Karls-Universität Heidelberg, Heidelberg, Germany
[94]Physik Department, Technische Universität München, Munich, Germany
[95]Politecnico di Bari and Sezione INFN, Bari, Italy
[96]Research Division and ExtreMe Matter Institute EMMI,
GSI Helmholtzzentrum für Schwerionenforschung GmbH, Darmstadt, Germany
[97]Saga University, Saga, Japan
[98]Saha Institute of Nuclear Physics, Homi Bhabha National Institute, Kolkata, India
[99]School of Physics and Astronomy, University of Birmingham, Birmingham, United Kingdom
[100]Sección Física, Departamento de Ciencias, Pontificia Universidad Católica del Perú, Lima, Peru
[101]SUBATECH, IMT Atlantique, Nantes Université, CNRS-IN2P3, Nantes, France
[102]Sungkyunkwan University, Suwon City, Republic of Korea
[103]Suranaree University of Technology, Nakhon Ratchasima, Thailand
[104]Technical University of Košice, Košice, Slovak Republic
[105]The Henryk Niewodniczanski Institute of Nuclear Physics, Polish Academy of Sciences, Cracow, Poland
[106]The University of Texas at Austin, Austin, Texas, USA
[107]Universidad Autónoma de Sinaloa, Culiacán, Mexico
[108]Universidade de São Paulo (USP), São Paulo, Brazil
[109]Universidade Estadual de Campinas (UNICAMP), Campinas, Brazil
[110]Universidade Federal do ABC, Santo Andre, Brazil
[111]Universitatea Nationala de Stiinta si Tehnologie Politehnica Bucuresti, Bucharest, Romania
[112]University of Cape Town, Cape Town, South Africa
[113]University of Derby, Derby, United Kingdom
[114]University of Houston, Houston, Texas, USA
[115]University of Jyväskylä, Jyvaskyla, Finland
[116]University of Kansas, Lawrence, Kansas, USA
[117]University of Liverpool, Liverpool, United Kingdom

[118]University of Science and Technology of China, Hefei, China
[119]University of Silesia in Katowice, Katowice, Poland
[120]University of South-Eastern Norway, Kongsberg, Norway
[121]University of Tennessee, Knoxville, Tennessee, USA
[122]University of the Witwatersrand, Johannesburg, South Africa
[123]University of Tokyo, Tokyo, Japan
[124]University of Tsukuba, Tsukuba, Japan
[125]Universität Münster, Institut für Kernphysik, Münster, Germany
[126]Université Clermont Auvergne, CNRS/IN2P3, LPC, Clermont-Ferrand, France
[127]Université de Lyon, CNRS/IN2P3, Institut de Physique des 2 Infinis de Lyon, Lyon, France
[128]Université de Strasbourg, CNRS, IPHC UMR 7178, F-67000 Strasbourg, France, Strasbourg, France
[129]Université Paris-Saclay, Centre d'Etudes de Saclay (CEA), IRFU, Départment de Physique Nucléaire (DPhN), Saclay, France
[130]Université Paris-Saclay, CNRS/IN2P3, IJCLab, Orsay, France
[131]Università degli Studi di Foggia, Foggia, Italy
[132]Università del Piemonte Orientale, Vercelli, Italy
[133]Università di Brescia, Brescia, Italy
[134]Variable Energy Cyclotron Centre, Homi Bhabha National Institute, Kolkata, India
[135]Warsaw University of Technology, Warsaw, Poland
[136]Wayne State University, Detroit, Michigan, USA
[137]Yale University, New Haven, Connecticut, USA
[138]Yildiz Technical University, Istanbul, Turkey
[139]Yonsei University, Seoul, Republic of Korea
[140]Affiliated with an institute formerly covered by a cooperation agreement with CERN
[141]Affiliated with an international laboratory covered by a cooperation agreement with CERN

[†]Deceased.
[‡]Also at Max-Planck-Institut fur Physik, Munich, Germany.
[§]Also at Czech Technical University in Prague, Prague, Czech Republic.
[‖]Also at Instituto de Fisica da Universidade de Sao Paulo.
[¶]Also at Dipartimento DET del Politecnico di Torino, Turin, Italy.
[**]Also at University College of Dublin, Dublin, Ireland.
[††]Also at Department of Applied Physics, Aligarh Muslim University, Aligarh, India.
[‡‡]Also at Institute of Theoretical Physics, University of Wroclaw, Wroclaw, Poland.
[§§]Also at Facultad de Ciencias, Universidad Nacional Autónoma de México, Mexico City, Mexico.